













NBSIR-1205(R)  
77-1205 (R)

E-(49-1)-3800-6  
Distribution Category UC-90g

# DEVELOPMENT, TESTING AND EVALUATION OF MHD-MATERIALS

Quarterly Report

for the period October - December 1976

H. P. R. Frederikse, T. Negas and S. J. Schneider

Inorganic Materials Division  
Institute for Materials Research  
National Bureau of Standards  
Washington, D. C. 20234

Date Published: December 31, 1976

PREPARED FOR THE UNITED STATES  
ENERGY RESEARCH AND DEVELOPMENT ADMINISTRATION  
Under Contract No. E(49-1)-3800

"This report was prepared as an account of work sponsored by the United States Government. Neither the United States nor the United States ERDA, nor any of their employees, nor any of their contractors, subcontractors, or their employees, make any warranty, express or implied, or assumes any legal liability or responsibility for the accuracy, completeness, or usefulness of any information, apparatus, product or process disclosed, or represents that its use would not infringe private owned rights."



Table of Contents

Page

ABSTRACT . . . . .	1
OBJECTIVES AND SCOPE . . . . .	2
SUMMARY OF ACHIEVEMENTS . . . . .	3
TASK G. Materials Program Coordination . . . . .	5
Program Review and Consultation US/USSR Cooperative Program	
TASK H. U-02 Phase I - Terminated June 30, 1976	
TASK I. Operational Design . . . . .	7
a. Viscosity of Coal Slags	
b. Electrical Conductivity	
c. Vaporization Studies	
TASK J. Corrosion and Diffusion . . . . .	19
a. Interaction of Seed with SiO <sub>2</sub> , etc.	
b. Diffusion of Potassium into Alumina	
TASK K. Materials Testing and Characterization. . . . .	24
a. U-02, ANL and AVCO programs	
b. Preheater Materials	
c. USSR Test at UTSI	
TASK L. Assessment of Downstream Components . . . . .	53
CONCLUSIONS. . . . .	60



ABSTRACT

Much time and effort during this first Quarter of FY 77 has been devoted to the coordination of electrode/insulator tests in various MHD-facilities. This involved close collaboration with a number of MHD contractors and sub-contractors with respect to the procurement of materials, the design of electrode/insulator assemblies, as well as the planning and information of actual running conditions. NBS is participating in a number of test series: the U-02 experiments, the ANL/Reynolds screening tests for U-25 electrodes, the recently initiated accelerated program of electrode testing in the MIT rig, as well as the AVCO-program on materials for slagging conditions. A considerable number of tested electrode assemblies were received by NBS; these are being analyzed and evaluated using optical microscopy, x-ray diffraction and SEM techniques. Valuable information was obtained concerning the durability of various electrode materials and the possible causes of degradation.

Two major problems addressed during this reporting period were:

- a. The fabrication of relatively thin layers (1-4 mm) of spinel, zirconia and chromite by means of arc plasma spraying.
- b. The joining of ceramics to metal-alloy lead-outs.

Because of the heavy emphasis on Materials Testing and Characterization (TASK K), work in other areas was somewhat reduced. Progress on other tasks included:

1. Viscosity was determined of some slag (Illinois #6) obtained from the UTSI MHD channel.
2. Additional data were obtained relevant to the interaction of seed and slag.
3. A thorough investigation was made of reaction layers on Corhart X-317 Ceramics exposed to flyash and seed in the test rig of the Fluidyne Engineering Corp.
4. A number of new and modified spinels were prepared and electrical conductivities of these materials were measured.



## Objectives and Scope of Work

The overall objectives of this program are to obtain chemical and physical definition of high temperature materials which have shown promise for use in coal-fired open-cycle MHD power systems. Major problem areas in which investigations will be concentrated are:

1. Characterization of coal slag and its effects on system components and performance at prototype temperatures.
2. Development of electrode materials which provide adequate performance over extended periods of time.
3. Insulating materials which limit thermal losses and are resistant to prolonged thermal and erosion effects.
4. Preheater materials which can withstand the operating modes of separately and directly fired operation.
5. Seed recovery methods from slag which are technically and economically feasible.
6. Phase equilibria and diffusion rates of seed in slag and the corrosive action of combination on system components and materials.
7. Durability of prototype MHD sub-systems.

The program is designed to contribute to the solution of these problems by providing much needed data on candidate materials and by evaluating test samples and structures that have been subjected to real or simulated MHD conditions. The activities are grouped under six tasks:

- G. Program Management Coordination (Assisting ERDA in coordination, planning and review of the various MHD-Materials Development Programs).
- H. U-02 Materials Testing and Characterization (Coordination of U-02 Test Activities, Phase I). (Terminated June 30, 1976).
- I. Operational Design Properties (viscosity, electrical conductivity, vaporization).
- J. Corrosion by Seed and Slag (phase equilibria, diffusion).
- K. Materials Testing and Characterization (test coordination, pre- and post-test analysis).
- L. Assessment of Steam Plant Components (corrosion resistance of metals and alloys).



Summary of Achievements - Oct.-Dec. 1976

(Completed Milestones - See Work Statement)

Progress of research and development in terms of the projected milestones of the NBS-ERDA contract are listed below. Because of new priorities and changes in the overall MHD program, certain objectives have been modified or replaced by more urgent goals:

- 1a. Conducted negotiation with USSR concerning materials testing U-02 (Phase I and II) and preliminary discussions concerning the Bypass U-25 experiments.
- 1b. Reviewed progress on US/USSR MHD Status Report.
- 2. Participated in ERDA-MHD reviews, planning sessions, etc.
- 4. Extended viscosity measurements on various coal slags.
- 16,19a. Determined the electrical conductivity of different coal slags and of various electrode materials (spinel,  $\text{LaCrO}_3$ ).
- 30. Obtained preliminary data on diffusion of Fe into pure spinel.
- 32. Prepared new spinels (also by means of arc-plasma spraying).
- 39a. Coordinated testing and pre- and post-test analysis of electrode/insulator assemblies tested in various MHD facilities (ANL/Reynolds, AVCO, MIT).
- 40a. Performed pre- and post-test characterization of various electrodes (Mg-Al-Fe spinel,  $\text{ZrO}_2$ ,  $\text{LaCrO}_3$ , etc.) by means of optical microscopy, SEM techniques, X-ray diffraction, etc.
- 42b. Assessed the degree of degradation of certain alloys (due to corrosion and oxidation) in a downstream MHD-environment.

An overview of the NBS-ERDA program schedule and accomplishments is presented in the form of a PERT-chart (Table A).



TABLE A. Program Schedule and Accomplishments

	FY 76				FY 77					
	Jul	Oct	Jan	Apr	Jul	Oct	Jan	Apr	Jul	Oct
<u>TASK G-Program Coord.</u>										
1 US/USSR Working Group on Materials										
Phase I		▽ test					△ final report			
Phase II						▽ test		→ final report		
Phase III, Bypass U-25										→
2 Planning, Reviews, etc.										→
<u>TASK I-Oper. Design Parameters</u>										
5,7 Viscosity of Slags, devitr.							▽			→
11 Vaporization										→
16,19 Electrical Conductivity, Slags, Spinels				▽			▽			→
<u>TASK J-Corrosion, etc.</u>										
20 Diffusion							▽			→
29,30 Corrosion (seed, slag, insulator)				▽						→
32 Preparation Spinels							▽			→
<u>TASK K-Materials Characterization</u>										
39a Charact. U-02				▽ Ph. I			▽		Ph. II	
b " ANL-Reynolds							▽		→	
c " AVCO					▽		▽			→
d " MIT										
<u>TASK L-Downstream Components</u>										
41 Data on K-Corrosion							▽			→
42 Alloy Assessment										→

▽ - MILESTONE  
 △ - COMPLETION





## Task G. MATERIALS PROGRAM COORDINATION (S. J. Schneider)

Program Review and Consultation Activities

S. J. Schneider participated in the regular ERDA-MHD staff meetings and in program review meetings (e.g., ANL U-25 program). The conclusions and recommendations resulting from these meetings are reflected in reports to ERDA or through direct consultation with ERDA staff.

NBS receives on a regular basis, MHD technical reports and proposals for review. During this period, NBS staff provided 36 such evaluations.

US-USSR Cooperative Program

## 1. U-25 Electrode Program

ERDA-MHD Division in early November 1976 initiated an accelerated program to identify viable electrode systems for possible application to the U-25 generator being developed through ANL. Participating organizations in the program (managed by ERDA) include NBS, Westinghouse, ANL, MIT, Battelle NW, Gilbert Associates. These groups act as the central focus for accomplishing specified programmatic functions.

The electrode systems receiving initial attention are reflected by the following Table (not all inclusive).

## ELECTRODE/INSULATOR/LEADOUT SYSTEMS\*

Base Electrode Material	Electrode Caps (oxides)	Electrode-Frame Interface	Insulator	Attachment
MIT spinel	ZR-Y	Mesh	MgAl <sub>2</sub> O <sub>4</sub>	Mechanical or
	ZR-Ce	Cermet	Y <sub>2</sub> O <sub>3</sub>	Solder
	Hf-Ce	Pin	(cooled/hot)	
NBS Spinel	ZR-Y	Mesh	MgAl <sub>2</sub> O <sub>4</sub>	Mechanical or
	ZR-Ce	Cermet	Y <sub>2</sub> O <sub>3</sub>	Solder
	Hf-Ce	Pin	(cooled/hot)	
LaCrO <sub>3</sub>	ZR-Y	Mesh	MgAl <sub>2</sub> O <sub>4</sub>	Mechanical or
	ZR-Ce	Cermet	Y <sub>2</sub> O <sub>3</sub>	Solder
	Hf-Ce	Pin	(cooled/hot)	
LaCrO <sub>3</sub>			MgAl <sub>2</sub> O <sub>4</sub> Y <sub>2</sub> O <sub>3</sub> (cooled/hot)	
Cu			Various	

\*Ceramic base systems designed for 2100 K electrode surface temperature and a range of operation of 1900 K - 2300 K.

NBS has the responsibility for overseeing the electrode development efforts involving cermet application. In addition to this, NBS will perform the attendant characterization of pre- and post-electrode systems from key screening tests.



2. Materials Tests in USSR and US

NBS coordinated the various activities related to the Phase II U-02 test conducted in Moscow during late September 1976. In addition to participating in the test, NBS staff are cooperating with Westinghouse and Battelle NW in the various post-test characterization efforts. The first draft of the final report is due in January 1977.

NBS also participated in the USSR materials tests conducted in October 1976 at UTSI. NBS staff will also aid in the characterization of tested samples.

3. US-USSR Status Report on MHD Materials

NBS, working with the USSR counterparts and ANL has reached a joint consensus on the initial draft of the report. It is expected that all details will be finalized by February 1977.

4. Steering Committee and Materials Ad-Hoc Working Group Meetings

S. J. Schneider participated in the October 1976 meetings in Moscow (as chairman of the materials group and member of the steering committee). The specific results of the meeting are reflected in the Protocol and trip reports. Basically, initial plans were formulated for testing activities to be carried out in the facilities of both countries during CY 1977 and subsequent years (tentative).

Item	Location	Date	Personnel	Activities
1. Steering Committee Meeting	Moscow	October 1976	S. J. Schneider, [illegible]	Discussed test results and future plans.
2. Materials Ad-Hoc Working Group Meeting	Moscow	October 1976	S. J. Schneider, [illegible]	Formulated initial plans for testing activities.
3. [illegible]	[illegible]	[illegible]	[illegible]	[illegible]
4. [illegible]	[illegible]	[illegible]	[illegible]	[illegible]
5. [illegible]	[illegible]	[illegible]	[illegible]	[illegible]
6. [illegible]	[illegible]	[illegible]	[illegible]	[illegible]
7. [illegible]	[illegible]	[illegible]	[illegible]	[illegible]
8. [illegible]	[illegible]	[illegible]	[illegible]	[illegible]
9. [illegible]	[illegible]	[illegible]	[illegible]	[illegible]
10. [illegible]	[illegible]	[illegible]	[illegible]	[illegible]



Task I. OPERATIONAL DESIGN PROPERTIES

a. VISCOSITY OF COAL SLAGS (W. Capps and D. A. Kauffman, Inorganic Glass Sec.)

Introduction

In an effort to furnish engineering data on the flow behavior of coal slags, NBS has been requested to measure viscosity-temperature relationships of slags furnished by several MHD contractors. These slags were from the combustion of Montana "Rosebud" and Illinois #6 coals. Some of this data has appeared in previous reports.

Slag Preparation and Viscosity Measurement

Viscosities were determined of a real slag and of a synthetic slag whose composition was chosen from the analysis of a real slag.

(1) Viscosity was determined from some slag obtained from the channel wall of the University of Tennessee Space Institute MHD test facility. This slag was from Illinois #6 coal. See Fig. 1. This slag is labelled NBS-K-983.

(2) A synthetic slag was prepared and the viscosity was measured. The composition was determined by an analysis of a real slag from Montana "Rosebud" coal. This slag is labelled NBS-K-795. See Fig. 2. The composition is as follows:

SiO <sub>2</sub>	42.10 weight %
Al <sub>2</sub> O <sub>3</sub>	19.50
Fe <sub>2</sub> O <sub>3</sub>	7.10
CaO	24.48
MgO	5.50
Na <sub>2</sub> O	0.21
K <sub>2</sub> O	0.10
TiO <sub>2</sub>	0.90

Viscometer Calibration

Due to the interest shown by a number of MHD contractors in viscosity measurement methods and viscosity data on both real and synthetic coal slags, it may be of use to have a brief description of the NBS Standard Reference Materials (SRM) which are used in calibration of the NBS high temperature viscometer and which are available to the public for this purpose.

NBS Standard Reference Materials 710 and 711 are the two SRM's used (out of the three available) for calibration of the NBS viscometer used on the coal slag program. SRM 710 is a soda-lime-silica glass and SRM 711 is a lead-silica glass. These are certified as to their viscosity-temperature



relationships (the  $\log_{10}$  viscosity of 710 from 2.00 to 12.00 over a temperature range from 1435 to 577 C; 711 from 1.90 to 12.00 over a temperature range from 1360 to 465 C).

These do not cover either the entire temperature range or viscosity range of interest to MHD studies but they cover broad enough ranges to determine the relationships between viscosity and the actual parameters being measured.

These two SRM's were used to recalibrate the NBS viscometer with a new platinum crucible and two different platinum spindles during this period.

### Liquidus Temperatures

Liquidus temperatures have not received much attention in reports characterizing different coal slags. Such data may prove to be very important because they will determine the lowest temperature at which the slags may be held without having them solidify because of crystallization. Most coal slags tend to crystalline rapidly once the temperature is low enough to permit crystal growth.

For purposes of discussion here the liquidus temperature is defined as that temperature above which no crystals can form or below which crystals will form if given sufficient time. Time, therefore, is an important consideration. Because different slags will crystalline at different rates any tabulation of liquidus data should indicate the time interval allowed during measurement.

Approximate liquidus temperatures can be inferred from NBS coal slag viscosity curves by referring to the lowest temperatures at which viscosities have been reported (actual data points). Crystallization was observed in each case at temperatures 10 to 25 degrees below the viscosity data point representing the lowest temperature reported.

If knowledge of more precise liquidus temperatures becomes important to the MHD program these could be determined from viscosity samples still on hand.

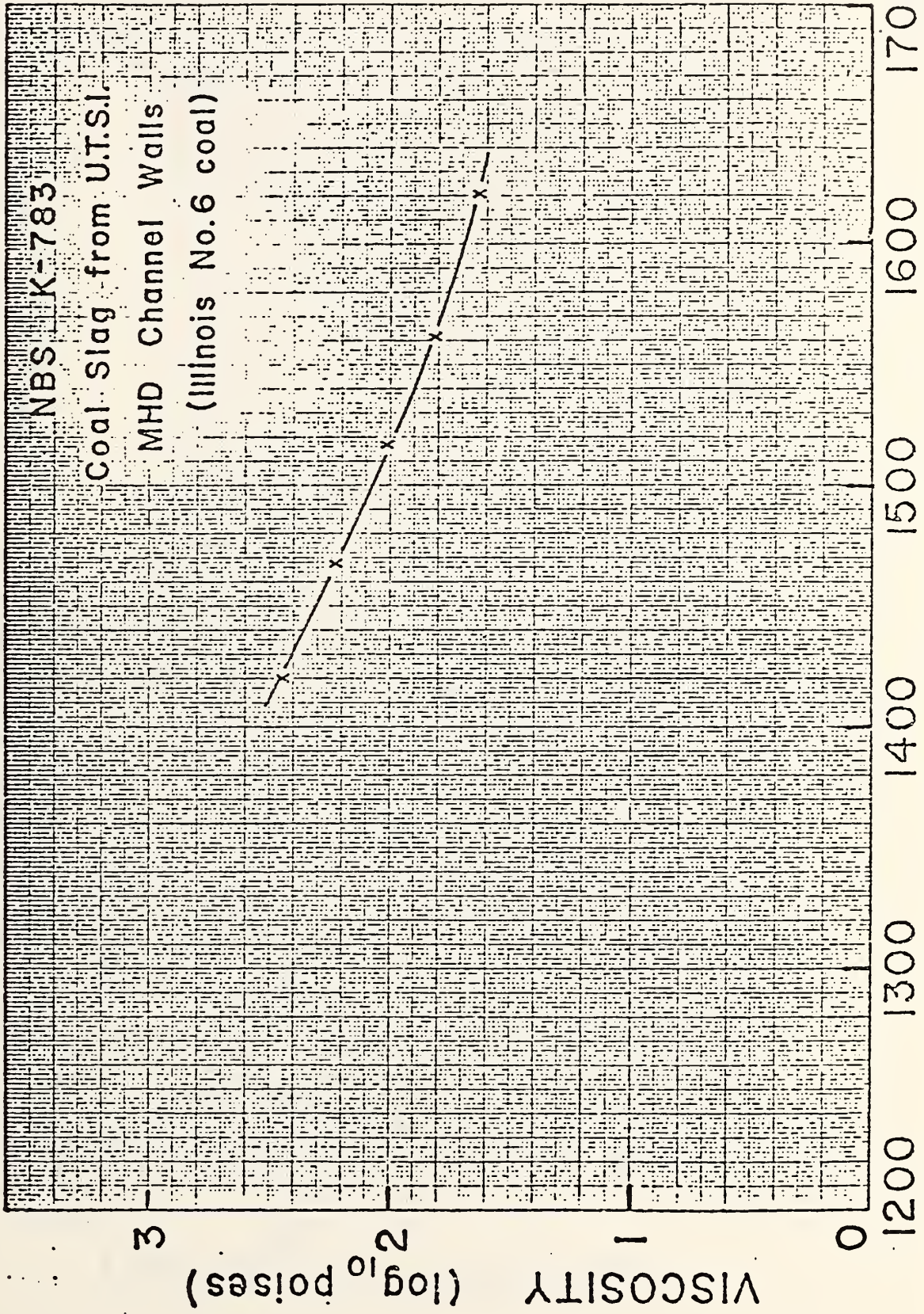
### Plans

1) Conclude experiments to determine the influence of  $\text{SO}_3$  on the viscosity of coal slags.

2) Attempt to incorporate factors for  $\text{SO}_3$  and  $\text{K}_2\text{O}$  into equations for predicting viscosity from slag composition.

3) Measure viscosity-temperature relationships of real coal slags for other MHD contractors on request.





TEMPERATURE (C)

Fig.1



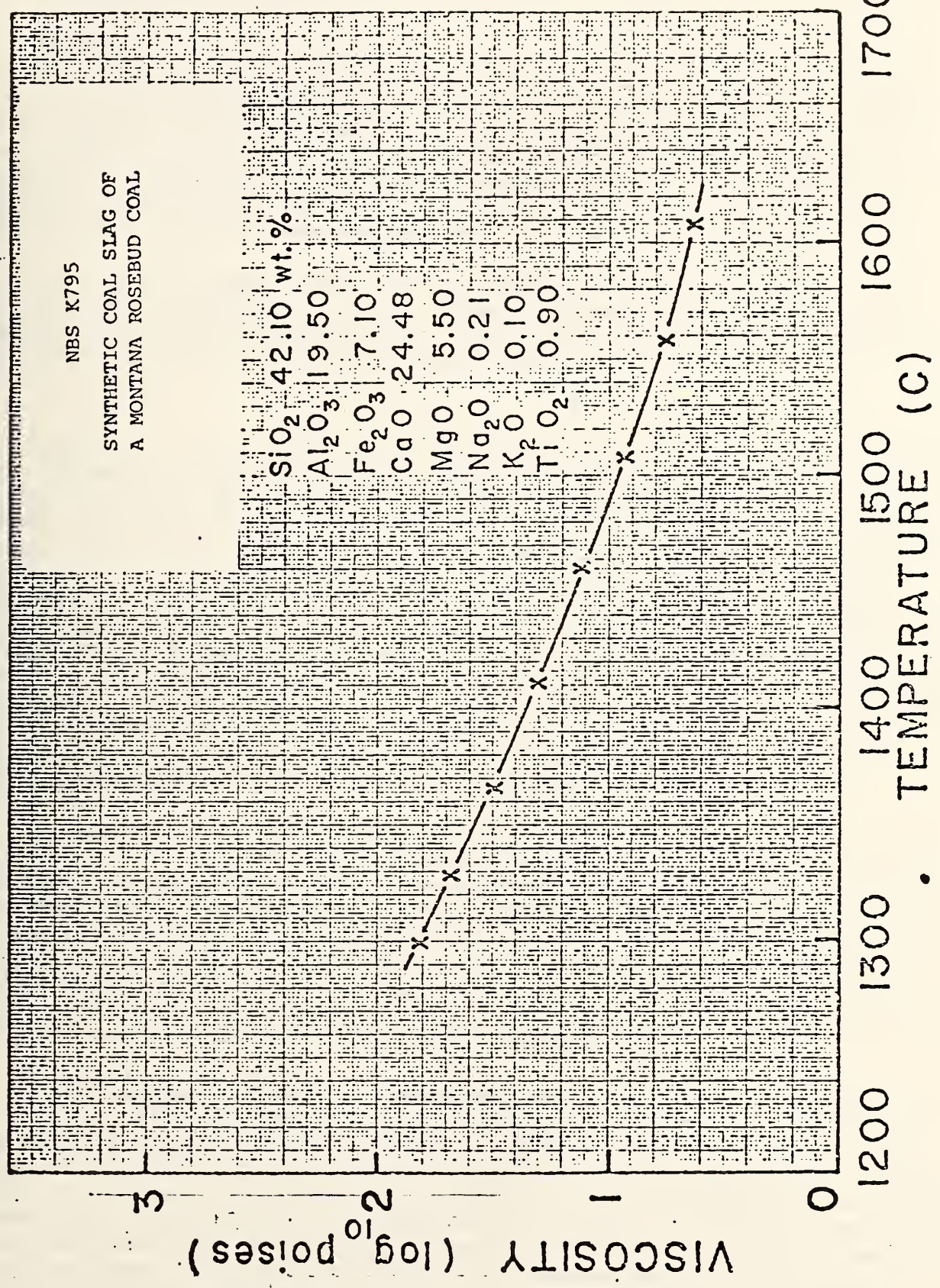


Fig.2



- b. Electrical Conductivity (A.J. Armstrong, W.R. Hosler, H.P.R. Frederikse, T. Negas and C. Olson)

### Spinels

Until now the Mg-Al-Fe-spinel, used as an electrode material, has been a solid solution between  $MgAl_2O_4$  and  $Fe_3O_4$  in the ratio 3:1 (MAFF-31). The U-02 (Phase II) test has shown that at the high temperature end, 1720 °C (or perhaps as high as 1820 °C), this material loses some iron oxide. Another feature of this spinel is its adequate conductivity at low temperatures ( $\sim 500$  °C). It might be preferable, however, to attach the spinel to the metal base at a still lower temperature.

Both aspects make it worthwhile to consider modifications of the MAFF-31 spinel: first, less  $Fe_3O_4$  in order to boost the melting point at the top surface of the electrode, and second, more  $Fe_3O_4$  to increase the conductivity of the bottom part in the temperature range below 500 °C.

X                    X                    X

Moderately dense ( $\sim 80-85\%$  of theoretical) slabs of Mg-Al-Fe-oxide spinels were prepared, in house, by conventional ceramic processing methods. Materials include the solid-solutions  $6MgAl_2O_4:Fe_3O_4$  and  $MgAl_2O_4:Fe_3O_4$  (mole %). The former should be more refractory but less conductive than  $3MgAl_2O_4:Fe_3O_4$ . The latter will be less refractory but more conductive. Samples were forwarded to Armstrong for electrical conductivity measurements. Our laboratory-scale preparations were intended to define potential problems prior to possible commercial preparations on a larger scale. In cooperation with an independent firm, billets of  $9MgAl_2O_4:Fe_3O_4$  were developed. However, billet density was low ( $\sim 80-85\%$ ) suggesting that final sintering temperature should be increased. This factor also was apparent in the laboratory-scale experiments. Laboratory scale experiments and attempts at commercial production suggest that the  $MgAl_2O_4:Fe_3O_4$  material will be more difficult to control due to excessive grain growth even at relatively low final sintering temperatures.

A review of the pertinent chemical literature revealed that  $NiAl_2O_4$ -based spinels may be promising materials in contact with silicate solutions. See, for example, Figures 2544-2546 in Phase Diagrams for Ceramists, The American Ceramic Society, 1969 Supplement.  $NiAl_2O_4$  has an unusually extensive primary phase field in the  $NiO-Al_2O_3-SiO_2$  system and is as refractory as  $MgAl_2O_4$ . The electrical properties of the material can be enhanced by additions of iron-oxides similar to the case of  $MgAl_2O_4$ . Anticipating processing requirements similar to  $MgAl_2O_4-Fe_3O_4$  spinels, we have ordered ceramic billets of two selected compositions for electrical measurements and slag corrosion studies.

Measurements of electrical conductivity were performed on 3 samples out of the four materials discussed above. The preparation of the samples has not yet been optimized as far as density and grain size is concerned. Fig. 3 shows the electrical conductivity of sample MAFF-91 ( $9MgAl_2O_4:1Fe_3O_4$ , density  $\sim 83\%$ ) as a function of temperature at 3 different partial pressures of oxygen. These results indicate that the conductivity is about two orders of magnitude lower than that of MAFF-31 ( $3MgAl_2O_4:1Fe_3O_4$ , see NBS-ERDA Quarterly Report #5, Sept. 30, 1976). Of course, this is to be expected because of the much lower iron content and the lower density. However, the conductivity at 2000 K ( $\sim 0.05 \text{ ohm}^{-1}\text{cm}^{-1}$ , slightly extrapolated) is probably adequate for an MHD electrode at this temperature. Measurements on higher density material will be made in the near future.



The conductivity of a sample of MAFF-61 ( $6\text{MgAl}_2\text{O}_4-1\text{Fe}_3\text{O}_4$ ), presented in Fig. 4 are somewhat better in this respect. Again, the density of this particular material is only around 80%: Less porous samples may show an appreciably higher conductivity.

The third sample is a solid solution of  $11\text{Ni}(\text{FeAl})\text{O}_4$  and  $1\text{MnAl}_2\text{O}_4$  (according to the manufacturer). The conductivity of this material (MAFF-11) (see Fig. 5 ) is very similar to that of MAFF 31.



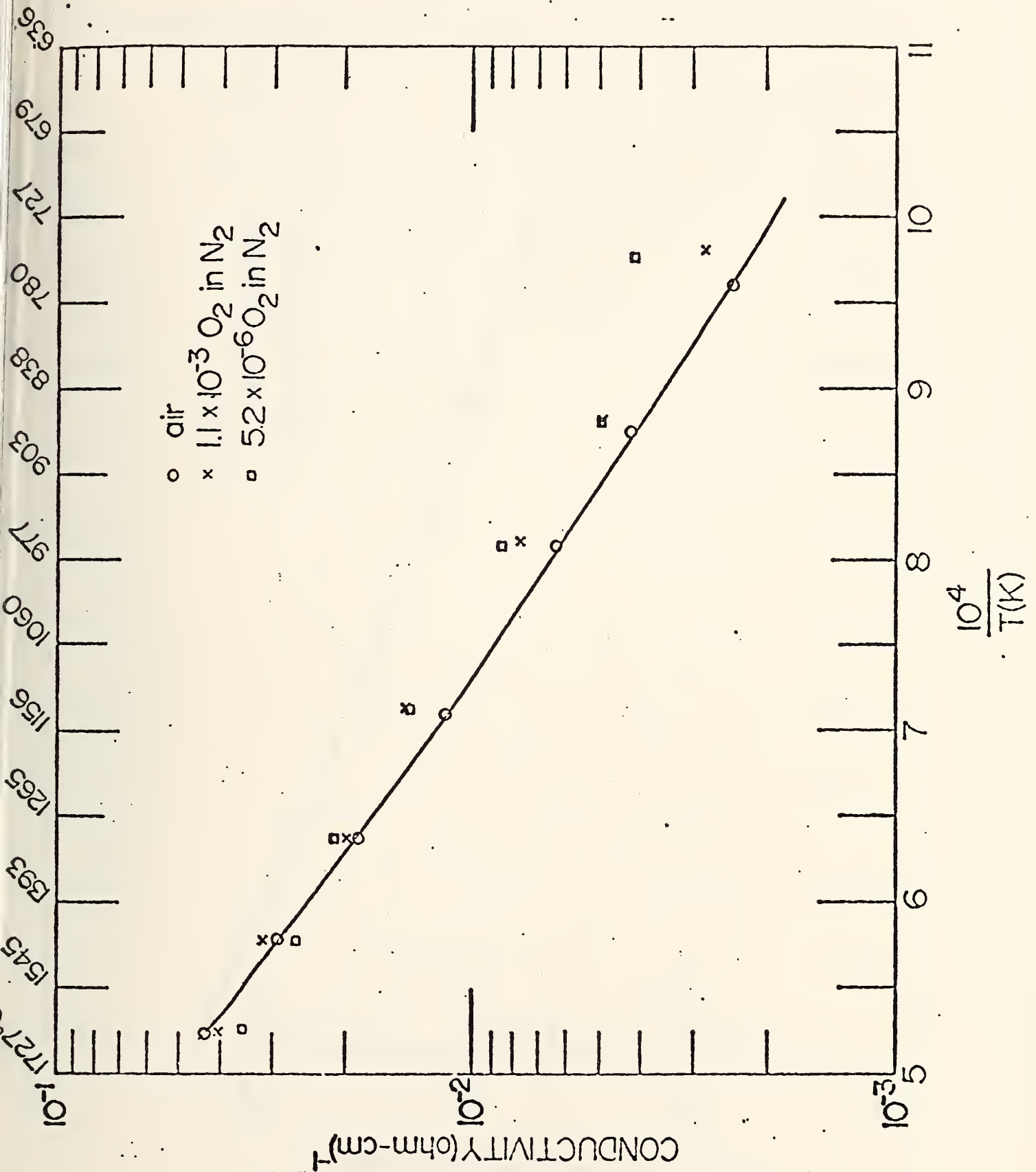


Fig. 3. Electrical conductivity of MAFF 91 ( $90\text{MgAl}_2\text{O}_4-10\text{Fe}_3\text{O}_4$ ) as a function of temperature at several partial pressures of  $\text{O}_2$ . Material prepared by Trans Tech Inc. and is 82.7% dense.



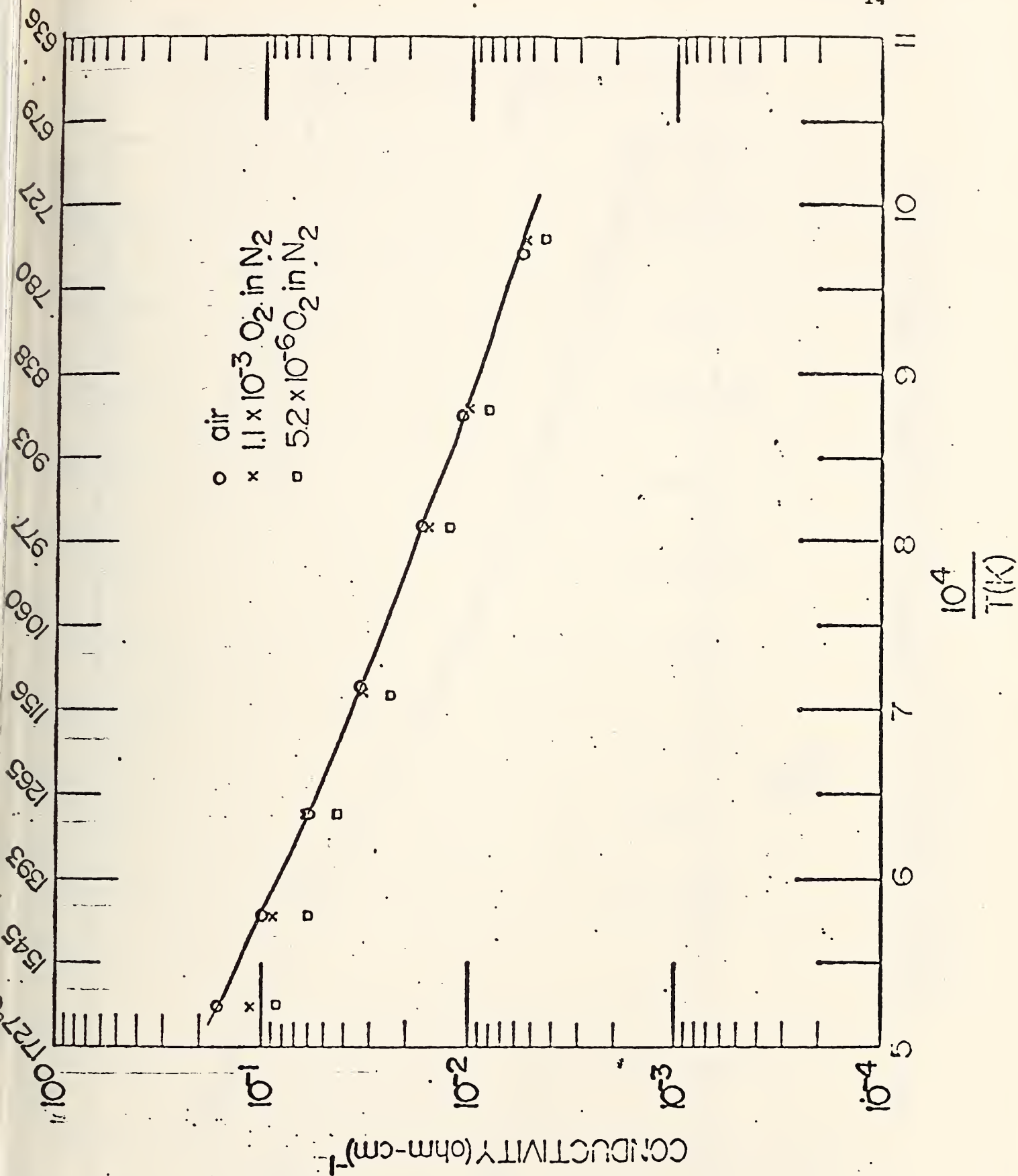


Fig. 4. Electrical conductivity of MAFF 61 ( $85\text{MgAl}_2\text{O}_4-15\text{Fe}_3\text{O}_4$ ) as a function of temperature at several partial pressures of oxygen. Material prepared at NBS and is ~80% dense.



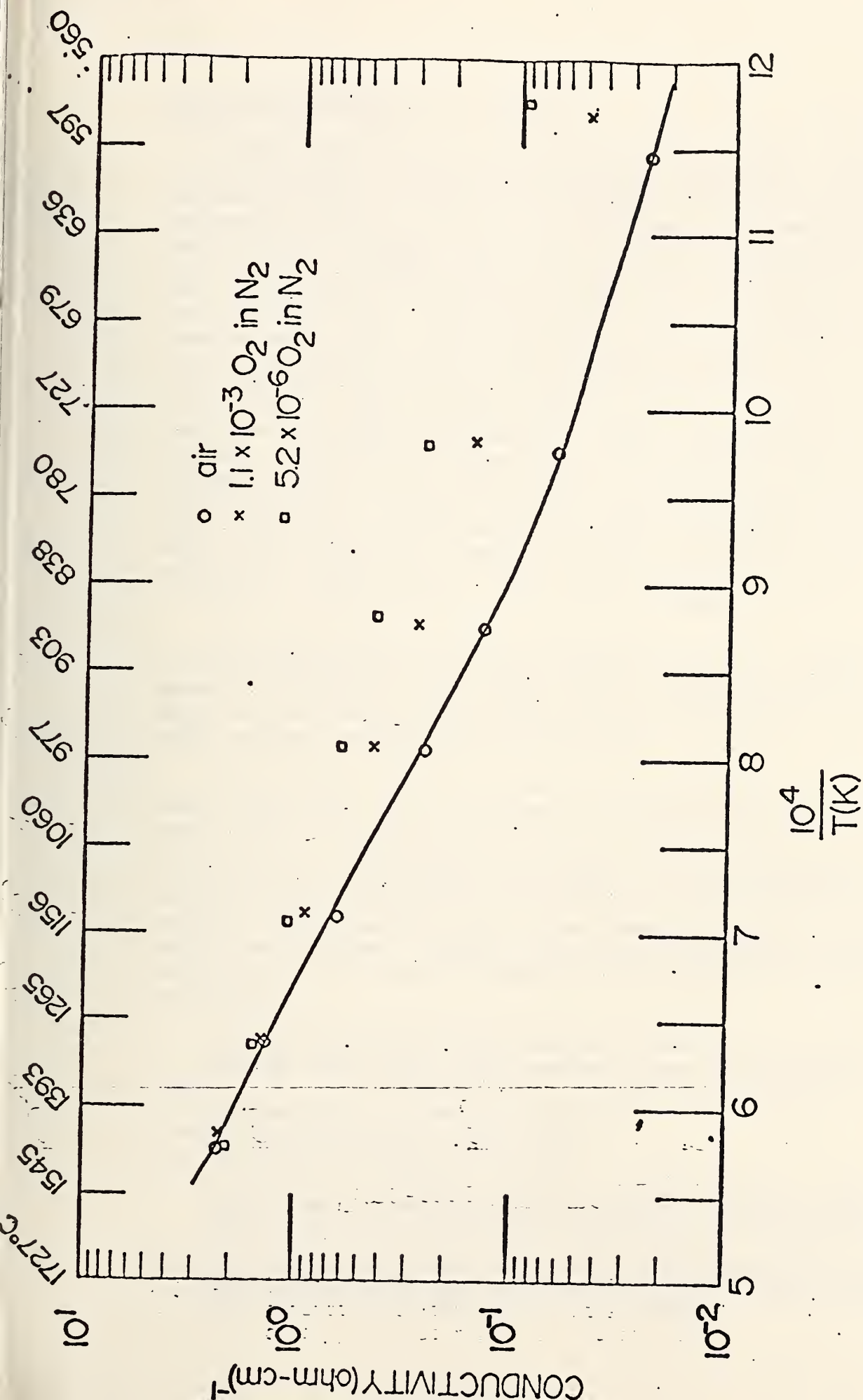


Figure 5. Electrical conductivity of approximately 11 Ni(FeAl)<sub>0.4</sub>-1 MnAl<sub>2</sub>O<sub>4</sub> as a function of temperature for several partial pressures of oxygen. Material prepared by Trans Tech Inc.



c. Vaporization Studies (E. R. Plante)

During this quarter vaporization measurements were continued on the K(g) pressure of K<sub>2</sub>O dissolved in SiO<sub>2</sub>. This work is considered important because of the role that silica plays in potassia-slag interaction. Efforts to study this problem in this laboratory have been outlined previously (1) and some results were presented at MHD meetings (2,3). Briefly, K(g) pressures were determined by a weight loss method using our Mettler TGA system and by mass spectrometry using a Bendix Time-of-Flight Mass Spectrometer. Differences in observed pressures in these measurements were attributed to hole size effects resulting from the use of different size effusion orifices. Data from the Mettler TGA work had been used (3) to estimate the interaction of potassia with silica. The implications of the mass spectrometric results were twofold. First, the Mettler TGA work yielded a thermodynamic estimate for the equilibrium concentration of K<sub>2</sub>O in a pure "silica slag" which is too high at lower temperatures and secondly, the failure to achieve equilibrium under relatively ideal Knudsen cell conditions with a sample area/escape area ratio of about 60 can probably be taken as fairly strong evidence that the equilibrium concentration of K<sub>2</sub>O in slag will not be attained except possibly for slag which has a long life on channel walls.

The measurements undertaken during this quarter were made in part to confirm the previous mass spectrometer measurements and in part to extend the composition range over which the measurements were made. They were made using a newly available Extranuclear mass spectrometer which employs a modulated molecular beam.

Since the K(g) pressure depends on the K<sub>2</sub>O concentration in the single phase melt, it is necessary to determine the amount of K<sub>2</sub>O vaporized as a function of time and temperature. This can be done if the initial or final composition of the sample is known by determining the weight loss of K<sub>2</sub>O which corresponds to a total integrated ion current  $\Sigma I^+ / T \cdot \Delta t$  where  $I^+$  is the ion current due to K<sup>39</sup>, T is the absolute temperature and  $\Delta t$  is a time interval during which the ion current was observed. The mass spectrometer instrument constant can be determined from these measurements provided the following assumptions are valid:

- (1) The mass spectrometer instrument constant is in fact constant;
- (2) The total weight loss observed is due to vaporization of K<sub>2</sub>O only;
- (3) The only K containing species being lost is K(g).

1. NBS Quarterly Report, June (1976).
2. L.P. Cook, E.R. Plante, T. Negas, R.S. Roth and C.D. Olson, Crystallization and Vaporization Studies on Synthetic Coal Slag Compositions, 15th MHD Symp., Philadelphia, PA, May (1976).
3. E.R. Plante, C.D. Olson and T. Negas, Interaction of K<sub>2</sub>O With Slag in Open Cycle, Coal Fired MHD, Sixth Intl. Conf. on MHD Electrical Power Generation, II, 211 (1975).



Assumption (3) is borne out by the mass spectrometric observations and thermodynamic considerations while assumptions (1) and (2) can be checked by measurement of the mass spectrometer constants in different experimental series and confirmation that the total  $K_2O$  loss is close to that expected. These assumptions were made for both the present measurements and those previously carried out using the Bendix spectrometer. For the sake of brevity, we will present here only a summary of the results obtained during this quarter using the Extranuclear mass spectrometer.

The data were fit to the equation

$$\log P_K = B_0 + B_1/T + B_2 \cdot N^2$$

where  $N$  is the mole fraction of  $K_2O$  in the melt and  $T$  is the absolute temperature. The separation of points into various series is somewhat arbitrary but was done to try to determine if the heat term would show a variation with composition. Points were separated into the same series if they had a common mass spectrometer calibration constant and if the range of composition was thought to be wide enough to give a reasonable determination of  $B_2$ .

The data are summarized in Table 1 which lists the series identification, the number of points, the composition range, the values of standard deviations and the standard deviation in log units of  $\log P_K$ . Examination of the values for  $B_0$  and  $B_1$  does not appear to reveal any systematic trend with composition and fit of all the data to a single equation in which the heat term is independent of composition appears justified. Over the composition range from .44 to .12 wt fraction of  $K_2O$  in  $SiO_2$  the equation,

$$\log P_K = 4.721 - 15624/T + 9.318 \cdot N^2$$

adequately represents the  $K(g)$  pressure over liquid solutions of  $K_2O$  in  $SiO_2$ . These weight fractions correspond to a range of mole fractions of .33 to .08. The temperature range for the measurements varied from 1300 - 1900 K. These measurements have a higher precision than any of those previously obtained in our laboratory.

At weight fractions below .20 and temperatures below about 1100°C crystalline tridymite would precipitate from the melt if equilibrium were established and the solution phase would become richer in  $K_2O$ . Thus far, we have not seen any evidence that this process is actually taking place. This is probably not too surprising since transformations in this system are notoriously slow.

#### Future Work:

The current measurements will be continued to test the  $K$  pressure dependence to as low a  $K_2O$  composition as practical and as a check on the  $K_2O$  composition variable. Work will be extended to more complicated slags. Of especial interest are slags containing both  $SiO_2$  and  $Al_2O_3$ .



Table 1

Least Squares Fit of K(g) Pressures  
over K<sub>2</sub>O-SiO<sub>2</sub> (z) Solutions

Series	No. Pts.	K <sub>2</sub> O wt. fraction	B <sub>0</sub>	S.D.	B <sub>1</sub>	S.D.	B <sub>2</sub>	S.D.	S.D.
1104	28	.439 - .404	4.482	.131	-15637	192	12.02	1.29	.041
1110	38	.403 - .344	4.790	.092	-15843	115	10.17	.66	.038
1115	26	.344 - .294	4.559	.076	-15485	98	10.42	.83	.034
1122	18	.293 - .265	5.349	.141	-15958	218	- 2.89	3.53	.047
1123	31	.265 - .211	4.491	.067	-15305	93	10.35	1.05	.029
1126	23	.211 - .166	4.784	.081	-15706	113	8.65	1.76	.030
1129	20	.166 - .119	4.735	.092	-15226	182	- 9.77	5.46	0.42
All	184	.439 - .119	4.721	.047	-15624	72	9.32	.13	0.57



Task J. Corrosion and Diffusion

a. Interactions of Seed with  $\text{SiO}_2$  and Other Oxides (L.P. Cook and C.L. McDaniel)

Work is continuing on a systematic study of phase relations in the system  $\text{K}_2\text{O}-\text{Al}_2\text{O}_3-\text{SiO}_2$ . Compositions investigated are indicated in Fig. 1. A synthesis diagram is given in Fig. 2.

Experiments along the join  $\text{KFeO}_2-\text{SiO}_2$  also continued.  $\text{KFeSiO}_4$  undergoes an undetermined reaction at  $945^\circ\text{C}$  and complete melting occurs at  $1215^\circ\text{C}$ . The tetragonal body centered phase  $\text{K}_{1+x}\text{Fe}_{1-x}\text{Si}_{1-x}\text{O}_4$  melts at  $1230^\circ\text{C}$ .

Another addition to the 3 component seed-slag system (K-Al-Si-O) that has been investigated is CaO. Data for subsolidus  $\text{CaO}-\text{K}_2\text{O}-\text{Al}_2\text{O}_3-\text{SiO}_2$  demonstrate that the  $\text{K}_2\text{O}$ -activity (-actually it is better to refer to the "chemical potential" of  $\text{K}_2\text{O}$ -) increases in the ternary system  $\text{KAlO}_2-\text{SiO}_2-\text{CaO}$  with increasing amounts of CaO. The occurrence of this effect in slags is suggested by K-pressures over synthetic slags and by actual MHD slag compositions.



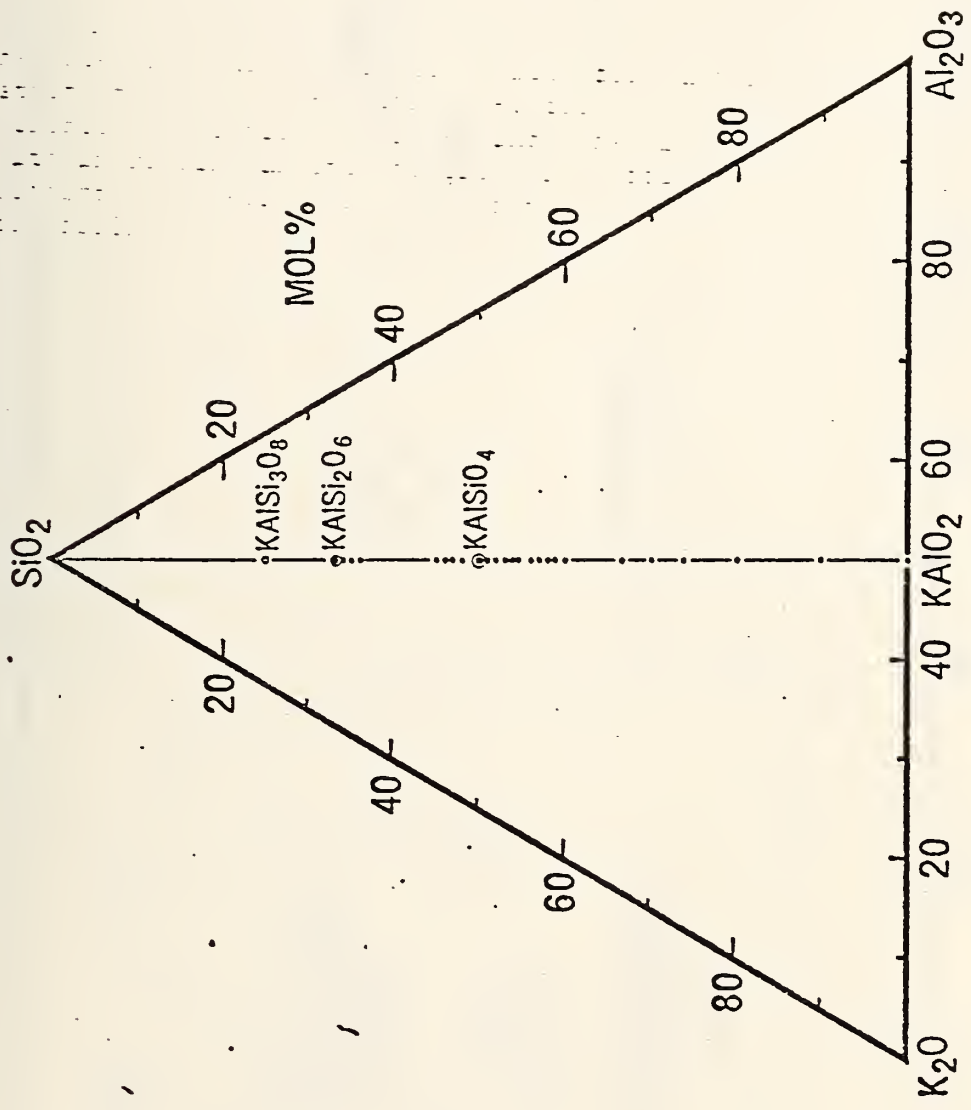


Fig. 1. K-Al-Si compounds in the ternary Phase diagram of the system  $K_2O-SiO_2-Al_2O_3$



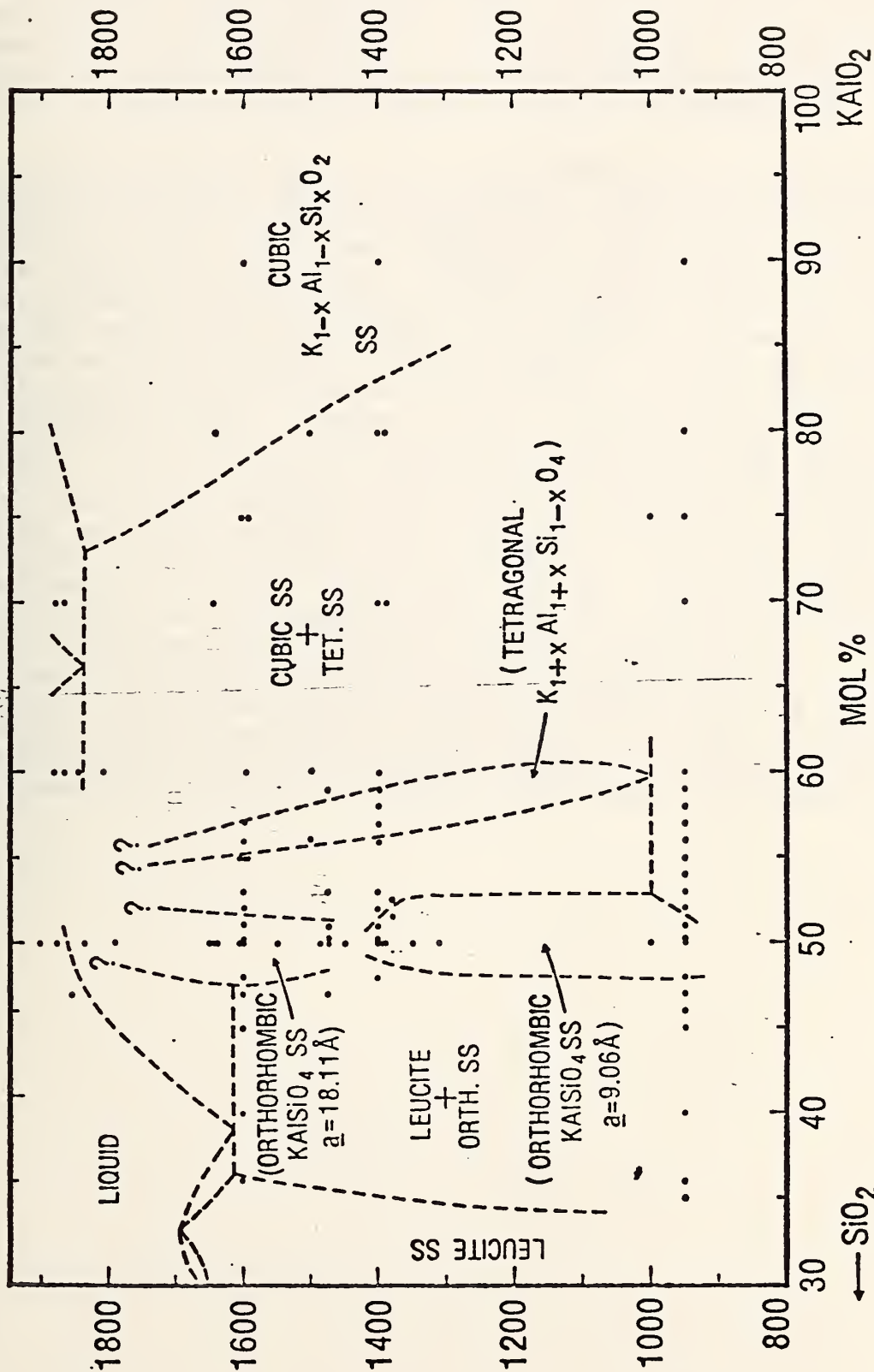


Fig. 2. Schematic phase diagram of the system  $\text{SiO}_2$ - $\text{KAlO}_2$  (<30 m/o  $\text{SiO}_2$ )



b. Diffusion of K into Alumina (J. R. Manning and E. N. Farabaugh)

To treat the problem of potassium diffusing into  $\text{Al}_2\text{O}_3$  ceramic we must make some basic assumptions. We assume a constant diffusion coefficient,  $D$ , in an infinite linear system which obeys Fick's second law for a one dimensional case:  $\partial c/\partial t = D(\partial^2 c/\partial x^2)$ . Upon application of the proper boundary conditions, which essentially are  $C = C_0$  at  $x \leq 0$  at  $t = 0$  and  $C = 0$  for  $x > 0$  at  $t = 0$  and a plane source, the solution to the diffusion equation is given in terms of an error function:  $C = C_0 [1 - \text{erf}(x/2\sqrt{Dt})]$ .

Thus, by determining  $C$ , the concentration as a function of  $X$ , the penetration into the ceramic, the value of  $D$  can be determined for known diffusion times at a specific temperature. The concentration profile of potassium in  $\text{Al}_2\text{O}_3$  (90% dense) diffused at 1400 °C for 90 hrs. was determined using an electron probe. Because of the porosity of the  $\text{Al}_2\text{O}_3$ , data were collected by scanning along a strip parallel to the edge of specimen and then moving into the interior of the specimen and scanning again. This method has been described in earlier reports. A 10  $\mu\text{m}$  beam was used and data were collected at intervals of 30  $\mu\text{m}$  from the edge. The data, as plotted on probability paper, is shown in Fig. 3. Data which fit the error function expression given above yield a straight line when plotted on probability paper. In Fig. 3, we see there are essentially two straight line segments. One which ends  $\sim 200 \mu$  from the surface and the second which begins there and continues to the end of the collected data. The first straight line segment yields a diffusion coefficient of  $5.7 \times 10^{-10} \text{ cm}^2/\text{sec}$ . The second yields a diffusion coefficient of  $\sim 1 \times 10^{-8} \text{ cm}^2/\text{sec}$  (at 1400 °C). The first diffusion coefficient would seem to be characteristic of a volume diffusion through the  $\text{Al}_2\text{O}_3$  grains while the second region could well represent a predominately grain boundary diffusion at a much faster rate. The data representing the volume diffusion has much less scatter than that which represents the faster rate which suggests that the K is not penetrating as uniformly in the faster diffusion region. The measurement of these diffusion coefficients of potassium into  $\text{Al}_2\text{O}_3$  ceramic represents achievement of a milestone under Task J (Corrosion and Diffusion).



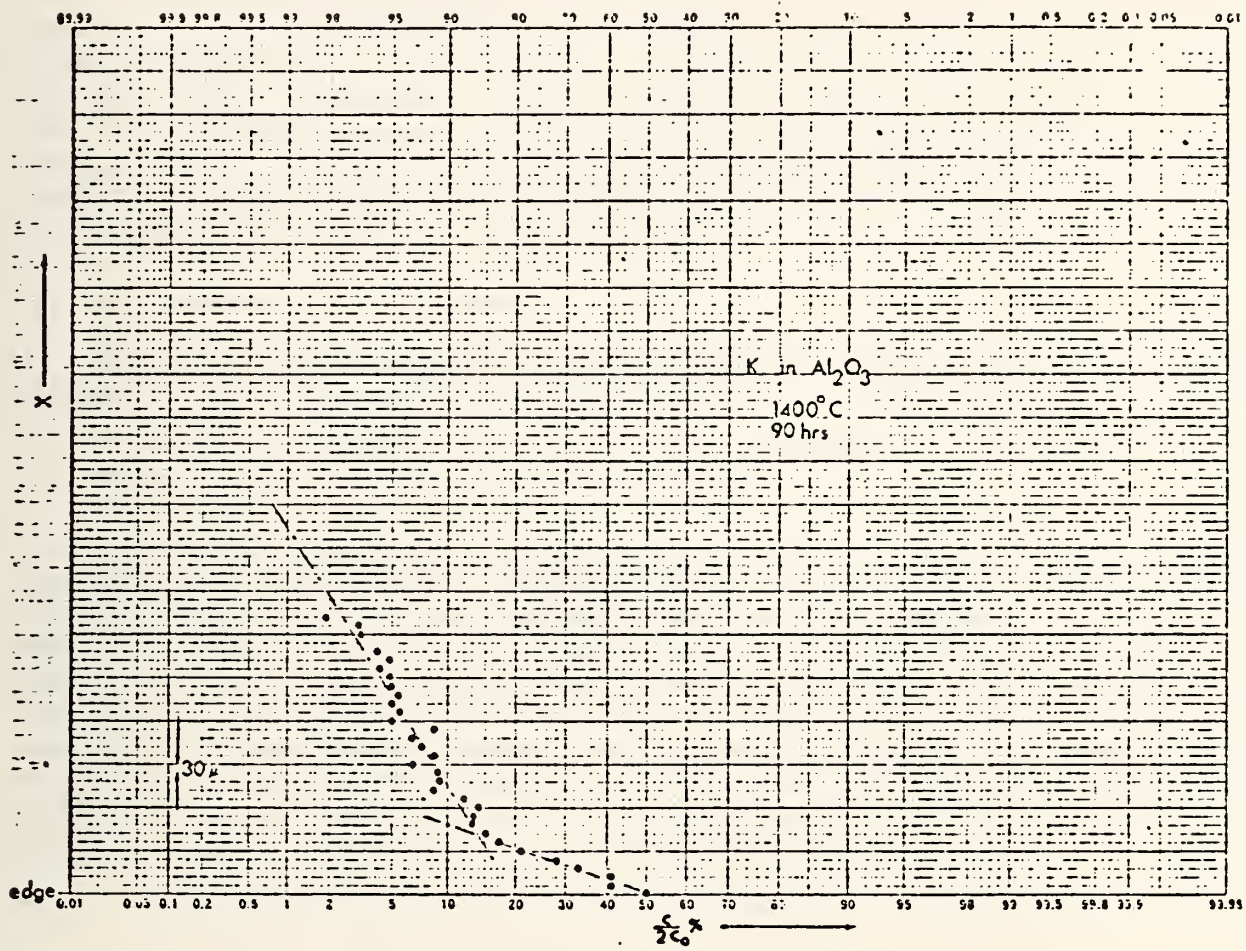


Figure 3. K concentration plotted on probability paper.

X = distance from the surface in 30 $\mu$  units.  
C = concentration at X.  
C<sub>0</sub> = concentration of K at surface.



## Task K. Materials Testing and Characterization

### a. U-02, ANL and AVCO programs

During calendar year 1976, NBS has become involved in a large number of tests of electrode/insulator assemblies and in the characterization of these assemblies. The conditions and objectives vary considerably from one test to the next. The materials tests in the Soviet U-02 facility are performed with clean fuel, heat fluxes of 15-20 W/cm<sup>2</sup> and for periods of 100 hrs. The ANL/Reynolds screening tests for U-25 electrodes are conducted in a small test rig for shorter periods of time, again with the clean fuel and heat fluxes of the order of 60-100 W/cm<sup>2</sup>. Experiments in the AVCO Mark VI are being run either with clean fuel or with simulated coal, large heat fluxes 100-300 W/cm<sup>2</sup>, and periods from 5 to 100 hrs. Because this report will discuss a number of characterizations of materials tested in different rigs and generators, it might be helpful to list the various tests for which NBS has performed the materials evaluation starting with the U-02 (Phase I) test of September 1975 (Table 1, Test 1 through 13):

#### 1. U-02 Phase I (W.R. Hosler)

The Final Report describing the materials evaluation and the conclusions derived from this test has just been published by ERDA (December 1976).

#### 2. U-02 Phase II, Analysis of Electrodes (T. Negas, W. R. Hosler, C. L. McDaniel, E. N. Farabaugh and A. Perloff)

La-Chromite and Spinel Electrodes (Test No. 2). The U-02, Phase II module was received, photographed, sectioned for analysis and re-photographed at NBS. Complete electrode/insulator assembly sections were forwarded to the Soviet side, Westinghouse Corp., and Battelle NW. We have completed our analyses, concentrating on the materials new to the U-02 program. These include LaCrO<sub>3</sub> ("doped" with MgO) and the iron oxide-containing spinels. Power X-ray diffraction combined with high magnification scanning electron microscopy (SEM) and energy dispersive X-ray analysis (EDX) were utilized as the dominant analytical methods. A final report to be transmitted to Westinghouse Corp is under preparation. A summary will be provided in our next Quarterly Report.

#### 3-5. ANL Screening Tests (for U-25 electrodes) in the Reynolds Test Facility

The Reynolds test rig (see Fig. 1) is a small 4" long channel fueled with propyl alcohol. Both electrode walls contain 8 electrodes (3/8" wide); on the anode side, the test electrode is No. 4 (T<sub>1</sub>) and on the cathode side No. 6 (T<sub>2</sub>). (See Fig. 1). The other electrodes are bare copper. The facility has no magnet. The surface temperatures of each of the test electrodes is measured with pyrometers (P<sub>1</sub> and P<sub>2</sub>). This way the state of the surface can be observed directly and continuously (visible area cross section ~3/16"). Other quantities measured are the temperature of the cooling water (which indicates the heat flux) as well as the applied cross voltages and interelectrode potentials.

A number of electrodes were tested in this facility between Aug. and Oct. 1976. Some details of these experiments are presented in Table 2. Rough sketches of the three electrodes tested in tests No. 3, 4 and 5 are shown in Fig. 2.



Table 1. Characterization of MHD-electrode/insulator Materials

Test and Specimen	Test Date	Rec'd at NBS	Analysis	Report
U-02 (Phase I) zirconia (+ceria)-clean	9/25/75 127 hrs.	10/75	Oct. 75-Jan.76	1. Express Report 2. Final Report 3. 15th MHD Symp.
U-02 (Phase II) ZrO <sub>2</sub> (+CeO <sub>2</sub> )-MAFF- hercynite-LaCrO <sub>3</sub> clean	9/21/76 100 hrs.	10/1/76	Oct.-Dec.76 Hosler-Negas Franti	
ANL/Reynolds hercynite-(MIT) clean	8/17/76	10/4/76	Oct.-Nov.'76 Farabaugh	NBS Quarterly Report 12/31/76
ANL/Reynolds Cermet-(U.C.) clean	8/22/76	10/4/76	Oct.-Nov.'76 Farabaugh	NBS Quarterly Report 12/31/76
ANL/Reynolds IN+ZrO <sub>2</sub> +Cu(AVCO) clean	9/10/76	10/4/76	Oct.-Nov.'76 Farabaugh	NBS Quarterly Report 12/31/76 AVCO Report 9/76
ANL/Reynolds ZrO <sub>2</sub> +st.st. (ANL) clean	10/76 (at least 10 hrs.)	11/29/76	in process	
ANL/Reynolds felt spinel (TN-NBS) clean	10/27/76 (HPRF) 25 hrs. total	11/29/76	In process	
ANL/MIT spinel (GE) clean	11/15/76	11/24/76	in process Negas	
ANL/MIT spinel-cermet(TT-NBS) clean	12/2/76 (WRH)	12/3/76	in process Negas	
AVCO IN-Cu(rail+buttons)(AVCO) slag	2/9/76	2/17/76	Feb.-April'76 Hosler Negas	15th MHD Symp. Petty Hosler Negas
AVCO wire mesh+spinel(A/TN) +ZrO (A-TN) st.st.+hercyn.(MIT) slag	Aug.'76	8/23/76 9/30/76	Sept.-Oct.'76 Negas	NBS Quarterly Report 12/31/76
AVCO -Cu+W-(AVCO) clean	Oct. 76	10/12/76	Oct.-Nov.'76 Negas	NBS Quarterly Report 12/31/76
AVCO grooved copper (AVCO) slag	Dec. 76 20 hrs.	12/8/76	in process Negas	



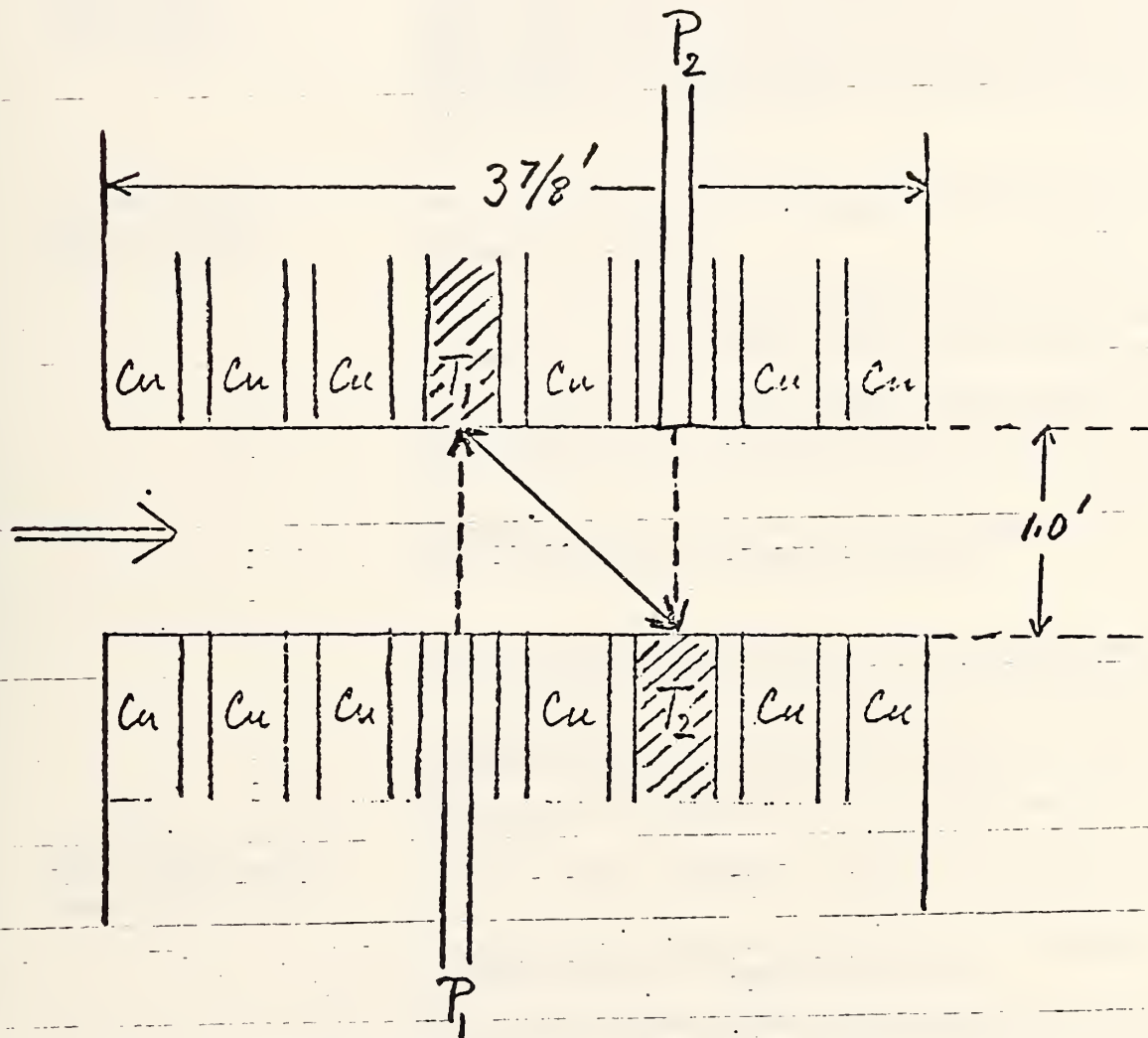


FIG. 1. Reynolds Test Rig.



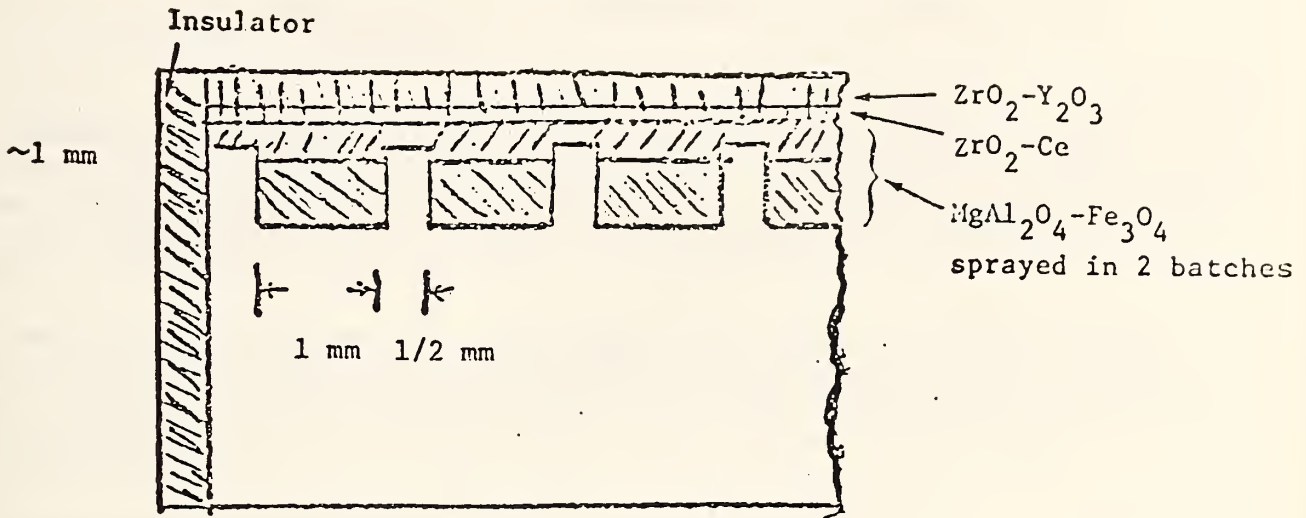
TABLE 2. ANL-REYNOLDS TESTS  
(supplied by ANL)

Aug. - Oct. 1976

TEST No.	Date and Running Time	ELECTRODES	TEST SUMMARY
3	8/17/76	M top layer: $ZrO_2(Y_2O_3)$ middle layer: $ZrO_2$ bottom layer: on top of grooved stainless steel	The test lasted 42 minutes and terminated in an emergency shutdown due to a blocked fuel nozzle. The fuel flow rate indicated that the test conditions reached about 25% of their design values. A restart was initiated and lasted approximately two hours and thirty minutes. This test was terminated at the end of the shift <u>without applying seed</u> . Fuel flow rates were about 50% of the design values. Later, test was started with duration of three hours and eleven minutes and terminated when the "anode" was observed to be badly eroded. The test section was removed and stored in the dry box for observation by ANL.
4.1)	8/22/76 14:22-16:20	U 83w/o $ZrO_2$ -17w/o $Y_2O_3$ graded to nichrome to INCO Alloy 600	This test reached a fuel flow rate corresponding to 25% of rate value and was terminated at the end of a shift. <u>No seed</u> or voltages were applied.
4.2)	8/23/76 15:10-17:50		Test was terminated using the emergency shutdown Mode due to failure of exit cooling system on segment #17. At shut down the fuel flow rate had been at 100% for approximately 1 hour.
4.3)	8/23/76 20:04-24:00 8/24/76 00:00-03:40		Test was terminated due to the improper voltage gradient down the channel. Ceramic was improperly cured and short-out the peg wall. Fuel flow was at 90% design values for approx. 5 hours and 6 minutes.
4.4)	8/24/76 21:53-24:06 8/25/76 00:00-07:03		Primarily a check-out test of the electrical system - 100% fuel flow design values for 6 hours and 57 minutes.
4.5)	8/26/76 13:46-23:39		Check out test of electrical system. Heat flux measurements and conductors. Fuel flow at design values for 9 hrs., 16 min.
4.6)	8/27/76 13:06-20:21		Diagnostic test. Fuel flow at design values. Test section was removed and placed in Hz fluid box for inspection, 7 hrs.
5.1)	9/10/76 16:00-24:00 9/11/76 00:00-24:00 9/12/76 00:00-20:31 9/12/76 00:00-20:31	A inconel buttons surrounded by castable $ZrO_2$ in copper "frames"	Heat transfer and conductivity tests. Design condition reached at 22:00. 24-hour at design condition - heat flux tests being conducted. Transverse voltage applied at 00.34 hr., 1 to 3 electrode current varied from 1.7 amps to 10 amps from Over a 6-hours period Aug current approximately 7 amp during this time. Fuel flow setting at design condition.
6		AN $ZrO_2$ on stainless steel	no details available
7	10/27-28/76 17:00-12:00 12:00-13:15 14:00-18:00	TN Arc plasma sprayed spinel on wire-mesh brazed to Hastelloy. (See NBS Quarterly Report 9/30/76).	Temperature raised to about 1400 °C, without applied voltage conditions, stayed very constant until noon (10/29). Heat flux ~60 W/cm <sup>2</sup> . Voltage applied and seed flow started J=1.5 A/cm <sup>2</sup> . After 1/2 hour some degradation visible. Arcing and hot spots. Voltage shut off - cooled down to room temperature.

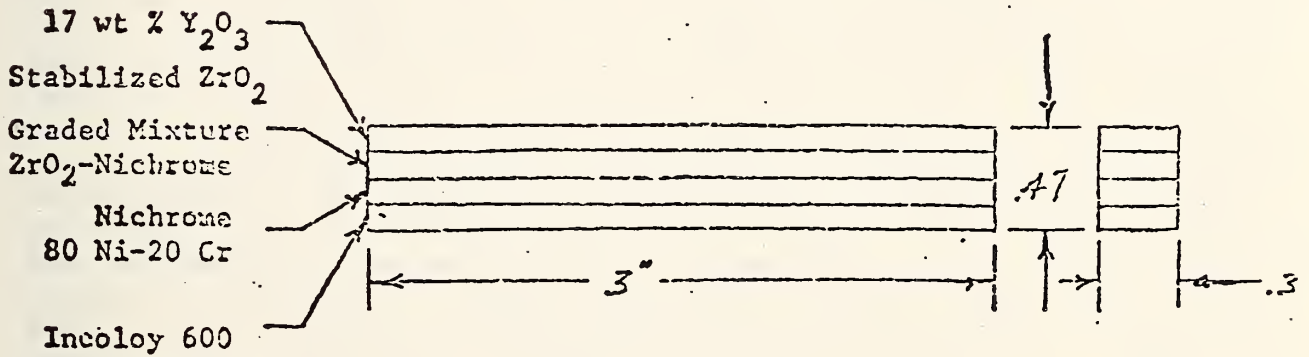


Test 3  
M



(B)

Test 4  
U



Test 5  
A

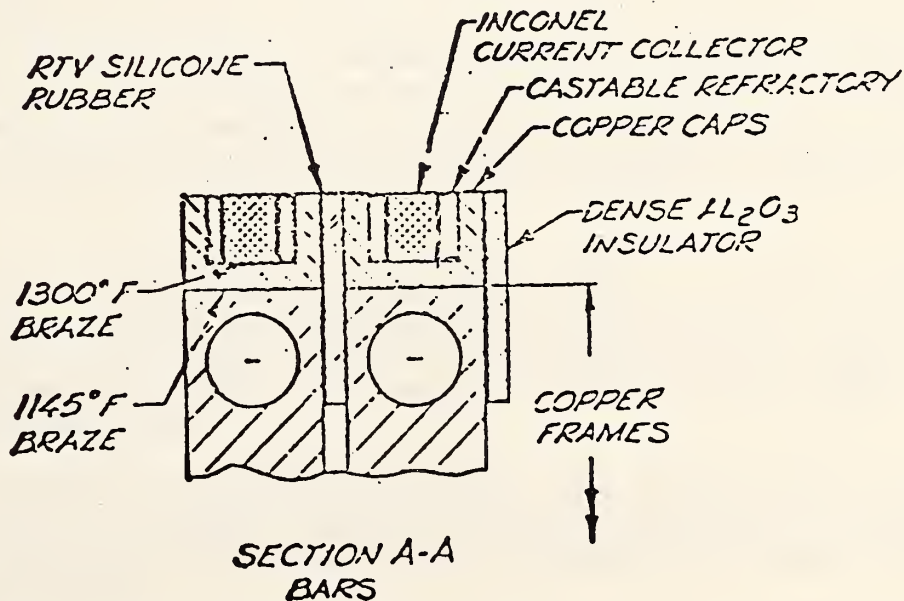


Figure 2. Sketch of electrodes tested in Tests 3,4, and 5 of the ANL/Reynolds program.



Examination of Electrodes Tested in the ANL/Reynolds Test Facility (Test Nos. 3, 4 and 5) (E. N. Farabaugh)

Material from Tests 3, 4 and 5 (Table 1) conducted at Reynolds was examined using SEM and EDX techniques. The samples examined were: Test 3, 11-101 (upstream anode), 11-201 (upstream cathode) and C-1 (samples from 05-202) and a piece of D-11 untested electrode material; Test 4, 01-102 (downstream anode) and 01-202 (downstream cathode); Test 5, 09-102 (downstream anode) and 01-202 (downstream cathode).

The electrodes were cut from the copper cooling block. Cross sections taken from near the middle of the electrode were used for specimens. In all cases, there was very little material left on the metal base of the electrode. The electrodes examined were chosen because they represented the most preserved material.

A. Zirconia-Hercynite-Stainless Steel Electrode (Test No. 3).

In sample D-11 (untested) there are four well defined layers of material on top of the 304 stainless steel base. In Fig. 3, the top layer -4- is the Zr-Y coating which has no Ce. Layer marked -3- has Zr-Ce and no Y. The next material is Fe-AlOxide (spinel). This appears to have been sprayed in two stages as shown in layers -2- and -1-. In the SEM micrographs a distinct boundary is evident and is the interface of layer 1 and 2. This interface appears to possess poor mechanical bonding and it has been noted that several of the electrode specimens broke apart along this interface. This breaking occurred both in the tested and untested material. Also observed in Fig. 3 are cracks in the spinel around the stainless steel stubs. These cracks were seen surrounding all stubs in the untested specimen. This indicates poor bonding of the spinel to metal in these areas. Cracks in the metal are also seen in this micrograph. A 200X micrograph of the stub (Fig. 4) reveals a typical crack. Note also the roughness of the top of the stub. Either the surface was eroded when the spinel was sprayed on, or the surface was roughened in expectation of achieving a better mechanical bond between the spinel and metal. (In some of these SEM micrographs some noise streaking is recorded on the print. This was due to a phosphor deteriorating during the examination time). It appears from these micrographs that the bonding between the various layers in the electrode could be better optimized. Each layer appears to be fairly uniform in microstructure, however. The major problem are the interfaces between two apparent spinel layers, the spinel metal interface and to a lesser extent the interface between the Zr-Ce-oxide layer and spinel. There is good apparent bonding between the Zr-Y-oxide and Zr-Ce-oxide layers.

Ca, Si and Al were found as the dominant impurities in the electrode material. To show the difference in layers 3 and 4 spectra was taken from each layer. Fig. 5 shows A the spectra taken near the top of the electrode showing strong Zr and Y lines. Spectra B was taken in layer 3 just above the spinel layer shows strong Zr and Ce lines no Y. The marker indicates the position of the Ce lines.

Higher magnification micrographs (1000X) were taken of the spinel, the Zr-Ce layer (above the spinel), and the Zr-Y layer near the top of the electrode. The Zr-Ce section appeared to be somewhat more porous than the rest of the electrode.



The first of the tested materials is shown in Fig. 6a . This is a 30X micrograph of the anode (11-101, test 3). Note that the electrode has cracked at two of the three interfaces indicated in Fig. 3 as being present in the untested material. Also we see the cracking around the metal peg which was also observed in the untested material. The porosity of the Zr-Y-oxide layer is greater than that of the spinel. Thus, the test has not changed the relative microstructure of the component materials. Figs. 6b and 6c are Fe and Zr maps of the same area; distributions of Y and Ce were measured also. The interface of the two Zr-based materials held up best and gives the appearance of a good solid bond. There does not seem to have been much movement of Zr, Y or Ce during the test since they are in rather well defined zones as shown by the mapping.

Fig. 7a is a 50X micrograph of the peg area shown previously. Again, we see the cracking at the corners of the peg and the roughness of the peg surface. Fig. 7b and 7c are Fe and Cr maps of the same area. There has not been much attack of the steel pegs since the Cr is well defined within the peg and the Fe in the peg is uniformly distributed. The Al map (not shown) indicates that some Al aggregation has occurred. The compounds formed have not been identified. This electrode, 11-101 test 3, was the most durable of all tested electrodes. It had by far, the most material left on top of the metal pegs and was in the best overall condition.

Fig. 8a is a 50X micrograph of the matching cathode (11-201 test 3). Figs. 8b, 8c, 8d, 8e, and 8f are Fe, Cr, Ni, Al and Zr maps of the same area. Obviously, the cathode has suffered much more in testing than the anode. The spinel material has been severely eroded away. The steel peg has also been attacked. The first three maps indicate movement of Fe, Cr and Ni. These effects are not seen in the anode. Again, there is compound formation involving the Al as seen by the Al map. It is seen that there is a decrease of Al in the region directly above the peg and heavier concentrations to the right and left of it. The Zr (and Y) maps show how little of the material was left on the electrode. There was little Ce left, not enough to map. This was typical of the cathodes. 11-201 was the best of the lot to examine.

The final specimen from test 3 was C-1. It was a layer piece which came off of 05-202. Fig. 9a is a micrograph of a cross section. Figs. 9b and 9c are Fe and Zr maps of the same area. This piece broke off at the interface lying in the flame sprayed spinel. This has been seen as a weakness in these electrodes. The zones of Fe, Zr (Y and Ce) are still well defined.

#### B. Cermet (zirconia-nichrome) electrode (Test No. 4).

In Test 4 the downstream anode (01-102) and downstream cathode (01-202) were examined. Fig. 10a is a 30X micrograph of the remains of the anode. Figs. 10b and 10c are Y and Cr maps of the same area. Only small amounts of Zr and Y are left in the wire gauze after the test. Some Si is present at the gauze-metal interface. Similar photographs were taken of the cathode. Even smaller amounts of Zr are seen and no Y could be detected in this cathode. About all that can be said about these electrodes is that nearly all the top layer of Zr-oxide was removed from the electrode during the test.

#### C. Metal (+zirconia) electrodes (Test No. 5).

Fig. 11a is a 50X micrograph of part of anode 09-102, the downstream anode in Test 5. In the micrograph the copper is on the right and the



center steel button is on the left. This is just one half of the electrode assembly. This anode material was very hard to polish and the castable around the center button tended to polish away. The cathode polished much more easily. Again, note that most of the material covering the metal part of the electrode is gone. Only relatively small amounts of material are left on either side of the center button. Fig. 11b is a Ni map of the same area. (Zr, Y and K maps not shown). Analysis of what looked like voids in the maps showed that these are regions in which the mounting compound has been exposed.

Other EDX work showed no Fe or Al concentrations in the castable material. SEM and EDX examination on the other side of the center pin (the more attacked side) yielded the same type of information, Zr, Y and K were found in the castable and no movement of metal into the castable was detected.

Fig. 12 is a 50X micrograph of part of the cathode 01-202, the downstream cathodes, of test 5. The copper is on the right and the center button on the left. The distribution of Ni, Zr, Y, K and Ca were mapped. Again, there appears to have been more reaction at the cathode. We see Ni aggregated now in the castable. There does not appear to be as much Y or K as in the corresponding anode. Also, we see a Ca concentration which was not seen in the anode. SEM and EDX examination of the other side of the center button yielded little new information. It must be noted, however, that on the other side only about 10% of the castable remained after the test. Ni, Zr, Y and K were detected in that remaining material.

X X X X

In a general evaluation of these tested electrodes it is difficult to make a detailed study since, in most cases, some of the interesting material is gone. In addition, very few untested electrodes were submitted, so that no valid comparisons could be made. The electrodes generally suffered degradation during the test and as a result it was sometimes difficult to prepare specimens without further damaging the electrode. Observations on the untested material suggest that better spraying techniques are necessary to withstand the rigors of operation.

In two cases 01-202 (Test 5) and 01-202 (Test 4) the metal of the electrode parted from the copper cooling block. The brazing failed in these cases. Typical brazes between cathode metal and copper are shown in Fig. 13, 09-102 (test 5), Fig. 14, 11-201 (test 3) and Fig. 15, 01-202 (test 5). Only in Fig. 15 is there any indication of a problem in bonding. Under higher magnification examination the good bonds showed good intimate contact with no voids or holes. With the exception of the two electrodes mentioned, all joining of electrode metal to copper held up well under testing.

## 6. ANL-electrodes

These electrodes were tested in the ANL/Reynolds rig in mid-October and were used mainly to check out the new conditions of the test channel with propyl alcohol fuel. Records of exact running times, temperatures and applied voltages have not yet been received.

C. ANL-electrodes

Fig. 13 is a 50X micrograph

of the brazing between cathode metal and copper.



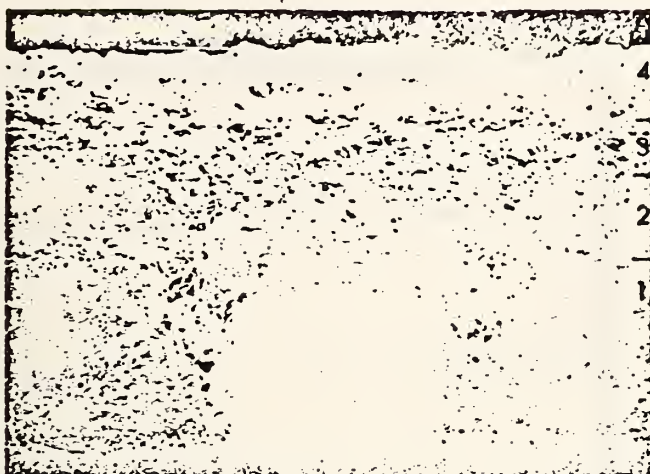


Figure 3. 30X SEM micrograph of untested material (D-11).

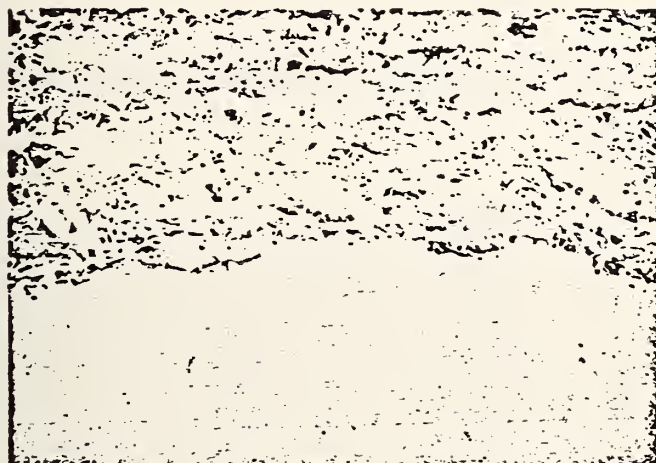


Figure 4 . 200X SEM micrograph of stainless steel stub.

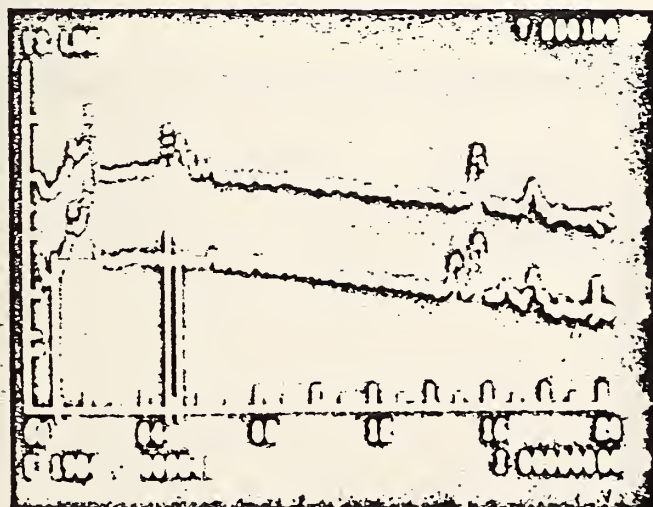


Figure 5. EDX Spectra from top two layers of electrode material.



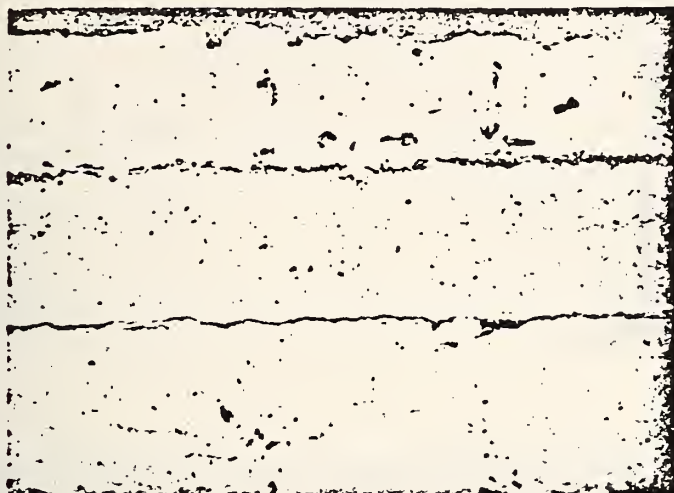


Figure 6a . 30X SEM micrograph of anode (11-101, test 3).

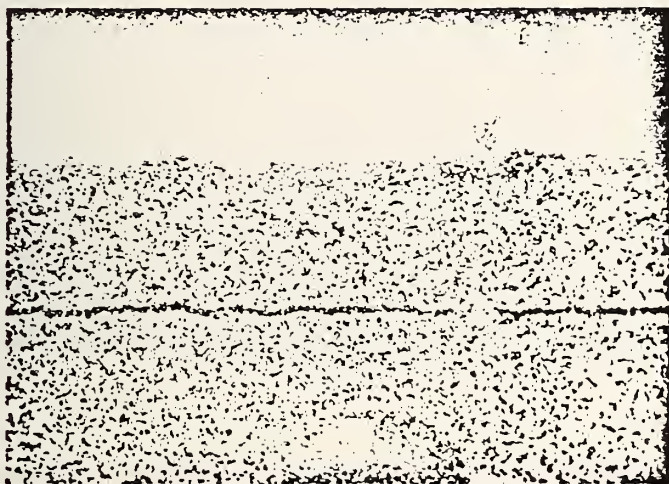


Figure 6b . Fe map of the same area



Figure 6c . Zr map of the same area





Figure 7a. 50X SEM micrograph of 11-101, test 3.

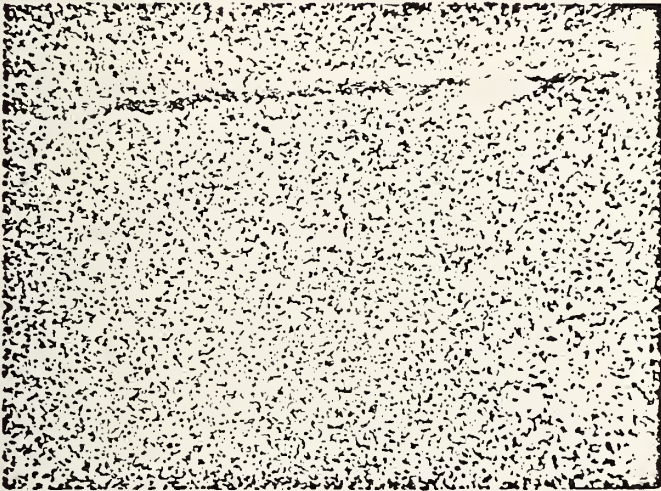


Figure 7b. Fe map of the same area

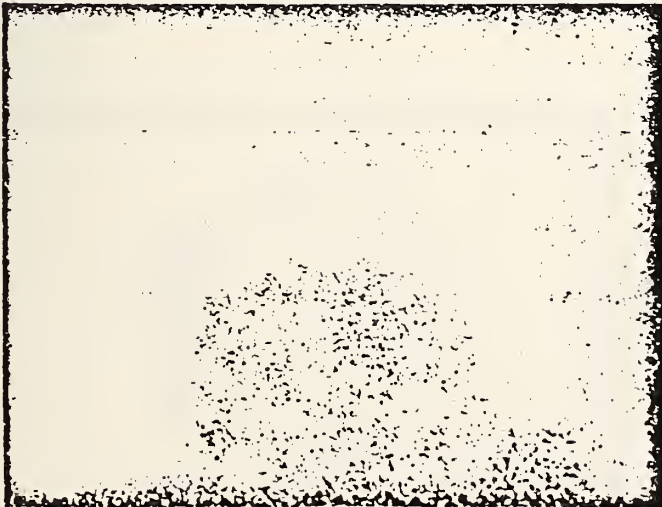


Figure 7c. Cr map of the same area





Figure 8a. 50X SEM micrograph of cathode 11-201, test 3.

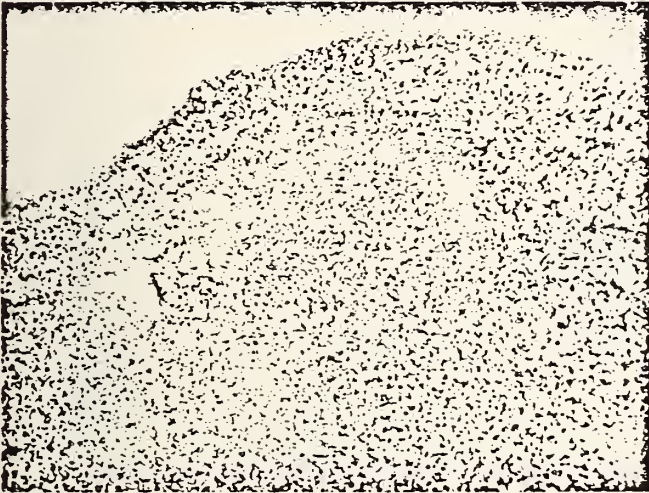


Figure 8b. Fe map of the same area

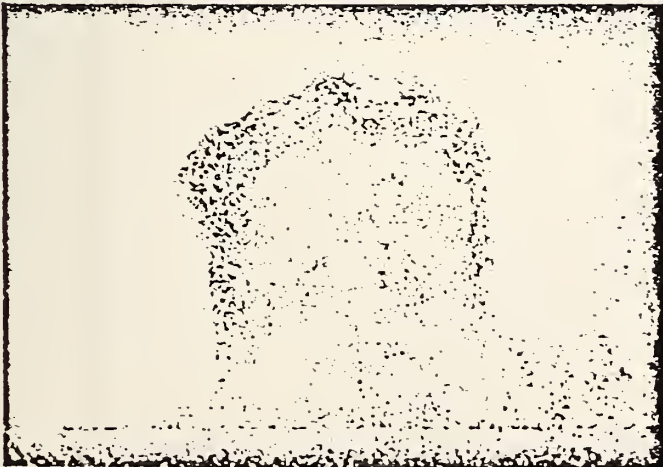


Figure 8c. Cr map of the same area





Figure 8d. Ni map of the same area



Figure 8e. Al map of the same area

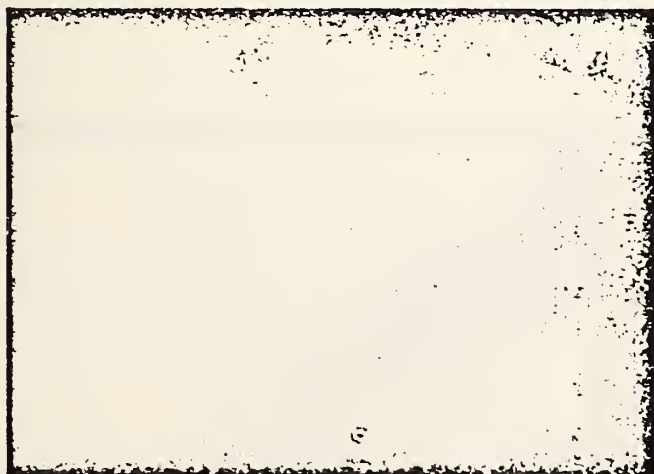


Figure 8f. Zr map of the same area



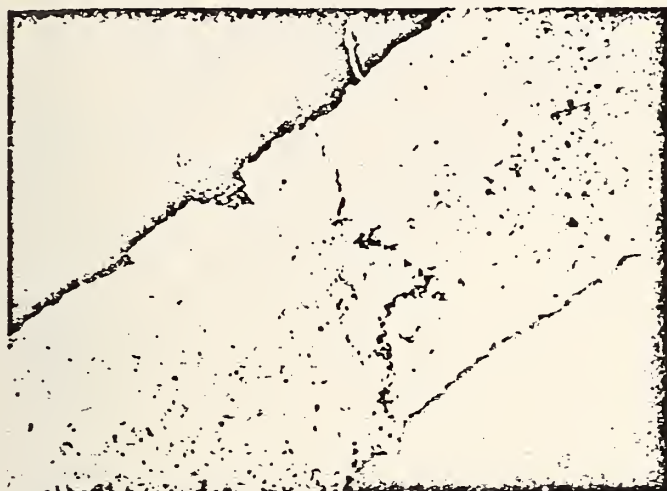


Figure 9a. 30X SEM micrograph of a cross section of specimen C-1.



Figure 9b. Fe map of the same area



Figure 9c. Zr map of the same area





Figure 10a. 30X SEM micrograph of anode 01-102, test 4.



Figure 10b. Y map of the same area

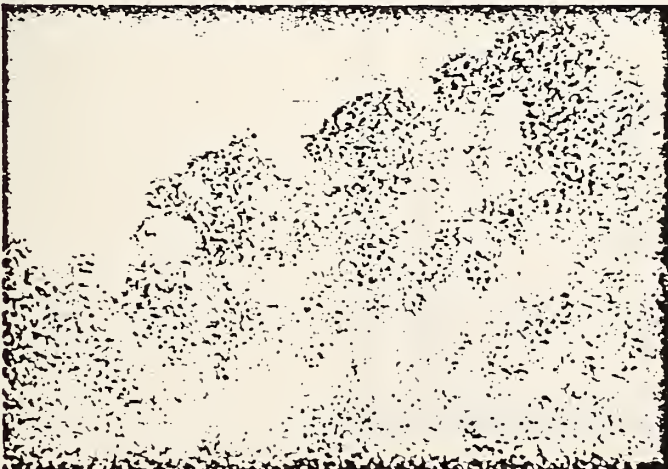


Figure 10c. Zr map of the same area





Fig. 11a . 50X SEM micrograph of anode 09-102, test 5.

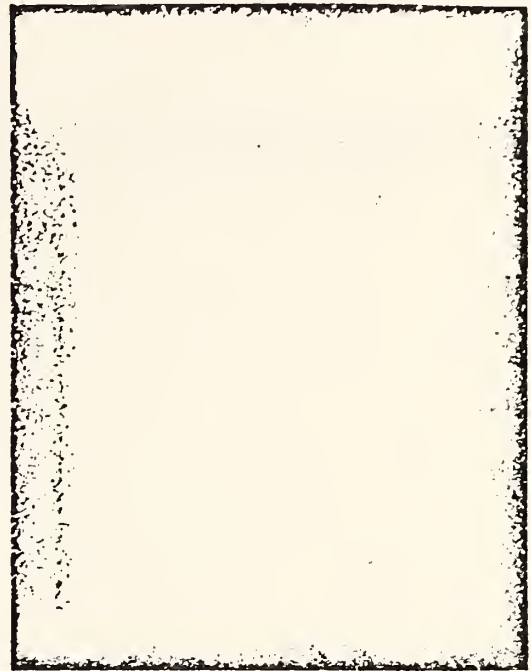


Fig. 11b. Ni map of the same area as

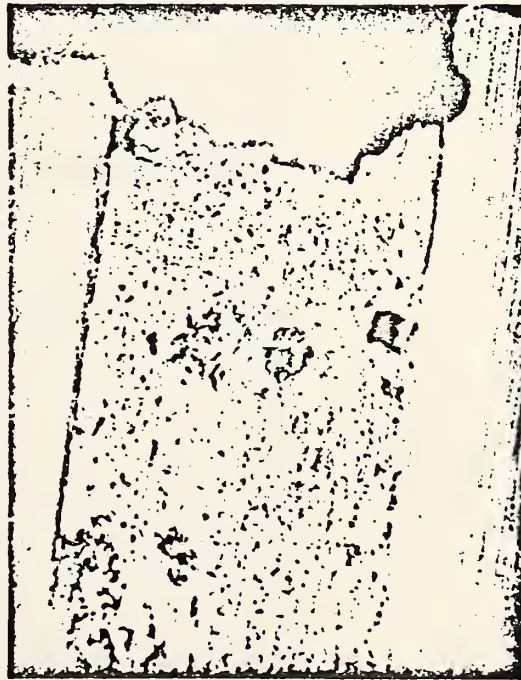


Fig. 12 . 50X SEM micrograph of cathode 01-202 test 5.





Figure 13. 50X SEM micrograph of brazed joint to cooling block, 09-102 (test 5).

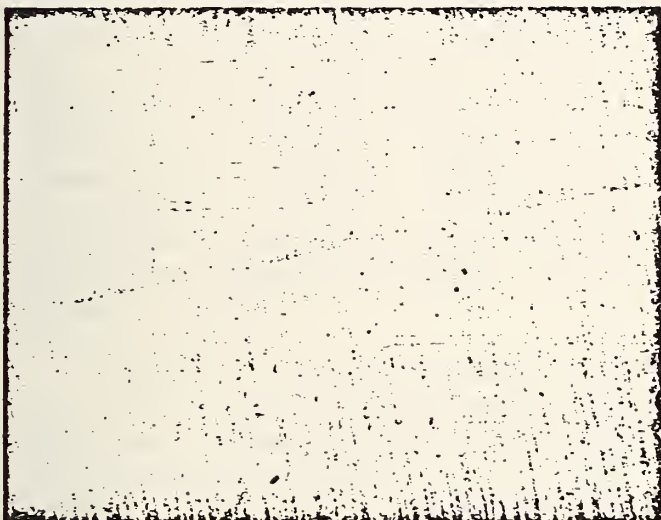


Figure 14. 50X SEM micrograph of joint in 11-201 (test 3).

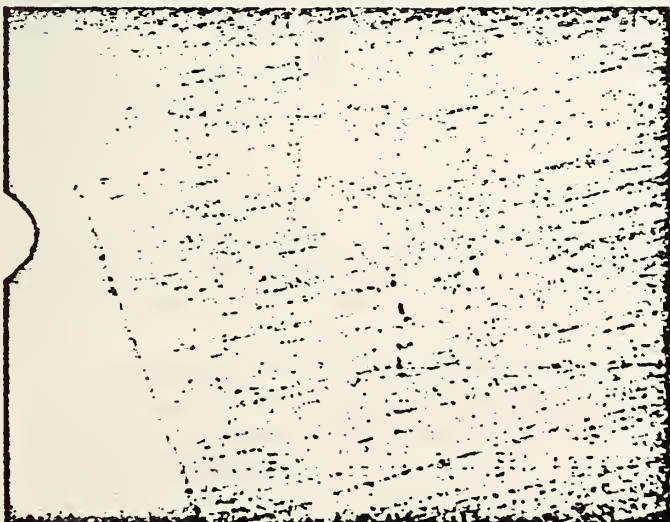


Figure 15. 50X SEM micrograph of joint in 01-202 (test 5).



## 7. TN-NBS Electrodes

The construction of these electrodes were described in the NBS-ERDA Quarterly Report of September 30, 1976. They consist of a 3.5 mm arc-plasma sprayed layer of MAFF spinel ( $3\text{MgAl}_2\text{O}_4 + 1\text{Fe}_3\text{O}_4$ ) on top of a 1.5 mm thick wire-mesh pad, which in turn is soldered to the watercooled copper holder. This electrode was tested in the ANL/Reynolds MHD facility in late October. It ran for about 15 hours under thermal conditions with a surface temperature of 1450 - 1500 °C, followed by 1-1/4 hours under current of 1.5 A/cm<sup>2</sup>. Characterization of these electrodes is in progress.

## 8. GE Electrodes

Analysis of these electrodes is in process. Details about the test are forthcoming from MIT, GE and ANL.

## 9. TT-NBS Electrodes

(The following is a short report of the test supplied by MIT):

These electrodes were tested in the MIT facility on December 2, 1976. The test plan called for a test of about one hour at a surface temperature of 1700 °C and a current density of up to 1.5 amps/cm<sup>2</sup>. The primary objective of the test was to test the cermet bond between the MAFF 31 spinel and the Hastelloy B substrate under thermal and electrical conditions similar to those expected in the U-25. The electrodes were designed for a heat flux of 100 watts/cm<sup>2</sup> at a surface temperature of 1700 °C and with an expected bond line temperature of 600 °C. The braze at the bond line was done with a relatively low-temperature solder. The electrodes had plasma sprayed inter-electrode insulation. Besides, NBS supplied additional insulator plates of pure  $\text{MgAl}_2\text{O}_4$  spinel and asked MIT to supply  $\text{Al}_2\text{O}_3$  plates for additional insulation on one of the surfaces.

Heating was done gradually, reaching a surface temperature of 1685 °C in one hour. The temperature was raised to 1725 °C before applying seed. Seed application lowered the surface temperature to 1700 °C. The surface was observed for 10 minutes for possible seed effects before applying electric current. Current at 0.45 amp/cm<sup>2</sup> was applied for 10 minutes. During this time the surface temperature rose to 1775 °C with hot spots at 1825 °C on cathode no. 2. The current was raised to 0.8 amp/cm<sup>2</sup> for 20 minutes. During this time incipient melting started to appear at a surface temperature of 1735 °C.(?) The current was subsequently raised to 1.15 amp/cm<sup>2</sup> for 10 minutes. During this time the coating on cathode no. 1 disappeared at a surface temperature of 1725 °C.(?) Consequently, the test was promptly terminated to save the other, partially damaged, cathode for analysis. The surface on the anodes was hardly damaged.

For the current densities used, the voltages on electrode 1 was higher than on electrode 2. This was likely due, in part, to the fact that the electrodes had separated from the copper blocks at the braze interface, resulting in different resistance across the junction.

Examination of the electrodes after the test revealed that they had separated at the brazed interface, the plate insulation had cracked normal to the electrode face, and the sprayed insulation had broken at the electrode-copper interface.



NBS Comment:

[Much of the damage might have been caused by the fact that these electrodes were not designed for the MIT rig. The length was 3" instead of 4-1/2" and hence, the flame had an opportunity to heat the ends of the electrodes excessively.]

10. AVCO Electrodes ("rail"- and "button"-type)

A report of this test and the materials characterization has appeared in the Proceedings of the 15th Symp. on Engineering Aspects of MHD (May 1976).

11. AVCO-Ceramic Electrodes (a, b. Zirconia & Mg-Al-Fe-spinel (Test 1a and b)

In the previous Quarterly Report some discussion was devoted to an analysis of AVCO anodes consisting of:

- a. wire-mesh (Fe, Cr, Al-alloy), sprayed  $ZrO_2$  ( $Y_2O_3$ ) plus slag, and
- b. wire-mesh, sprayed spinel ( $3MgAl_2O_4:Fe_3O_4$  solid solution) plus slag.

Figures 16 and 17 (100X), respectively, show typical cross-sections. The upstream end (left) of each electrode was subjected to current concentration, heating, and oxidation, in situ, of the wire-mesh. Although most of the  $ZrO_2$  ( $Y_2O_3$ ) [discontinuous, white patches in Fig. 16] reacted/dissolved in the slag, the wire at the downstream end remains practically intact suggesting minimal current activity and/or lower temperatures. Furthermore, the upstream wire-mesh in Fig. 16 also is characterized by "pockets" of "invading" slag components. In contrast, the spinel layer (dark grey zones above wire in Fig. 17) suffered recession (original thickness, ~1 mm), yet forms a continuous layer above the wire-mesh. Oxidation products (light grey) of the wire are retained within this layer. Possible current channeling is apparent at the downstream end (right) as suggested by the oxidation of the underlying wire.

Within each electrode several noteworthy interfaces developed during this short term test. In Fig. 16, a continuous layer of crystalline slag covers the lower zone of wire-mesh plus  $ZrO_2$  ( $Y_2O_3$ ) and metal oxidation products. This layer extends upward to a well-defined porous zone midway through the cross-section. Above this zone is a continuous layer of glassy (molten during operation) slag. The porous interface between molten/crystalline slag may suggest gas evolution (probably oxygen) at the anode. Also, a crystalline, presumably resistive, layer of slag overlies the wire-mesh; current channeling is evident only at the upstream end. As seen in Fig. 17, a sharp, continuous contact exists between slag and the lower zone of wire-mesh plus spinel and metal oxidation products. At the upstream end, this interface is not porous and consists of glassy (molten) slag directly on wire-plus-oxides. An intervening, crystalline slag layer is not evident. Approximately half-way across the electrode, a highly porous but poorly defined interface begins and extends to the downstream end. Crystalline slag exists below while glassy slag occurs above this interface, similar to the situation in Fig. 16. It seems apparent that the controlling factor in the development of these interfaces is the chemical nature of the original, sprayed ceramic oxide. Assuming a fixed initial slag composition and, initially, nearly identical temperatures at the upstream portion of each electrode, incorporation (reaction, solution, etc.) of refractory  $ZrO_2$  ( $Y_2O_3$ ) by the slag should not lower the liquidus temperature of that slag, i.e., crystallization can occur within the temperature regime wherein the initial slag composition normally is molten. Incorporation of spinel, and especially the iron-oxide component, operates in the opposite manner.



The liquidus (or molten range) of slag actually is extended to lower temperatures. In Fig. 17, it is precisely at the hotter upstream end where most of the original spinel was incorporated that the slag layer remains molten. A zone of the crystalline slag occurs only toward the downstream, presumably cooler, end where less spinel has been incorporated.

The observations above are noted for several reasons. For, at least, short term durations the properties of a slag can be altered, possibly beneficially, by semi-sacrificial ceramic oxide layers. Care must be extended, however, in the choice and design of these materials. For example, iron-containing oxide coatings when incorporated with slag plus seed could lower, even temporarily, the molten range of slag plus seed to excessively low temperatures. Thick, highly conductive, low temperature, molten slag could bridge insulation and lead to interelectrode breakdown.

### c. Hercynite (Test 11c)

We also received a cathode operated for 30 hr with slag/seed. It consisted, originally, of stainless steel having a ridge and groove surface onto which a coating of an Fe-Al-oxide spinel (composition unknown) was applied. Fig. 18 (100X) illustrates a typical cross-section. Higher magnification micrographs and EDX data are available. A flat polished surface could not be maintained (shown by the irregularities in Fig. 18) as the electrode was saturated by potassium salts which hydrated and "bled" during handling.

The electrode apparently suffered from excessive heating particularly at the downstream end (right side) wherein the stainless steel suffered extensive recession via oxidation. The remaining stainless steel pins (grey) on the upstream side also are being subjected to oxidation but at a slower rate. Oxidation products (Fe/Ni/Cr-oxides) surround these pins. Slag components including K have replaced entirely the pre-existing spinel ceramic. Dark grey areas between the stainless and slag and the zones containing "bubbles" above the slag consist of epoxy.

## 12. AVCO Electrodes (T. Negas)

### Cu-W-electrodes (Test No. 12)

During this quarter we received an anode fabricated from a metal composite consisting of a mixture of Cu plus W metals (presumably sintered W impregnated with molten, Cu, or W/Cu metals sintered above the melting point of Cu, nearly 1:1 proportions). This material, operated for 20 hr. under clean fuel/seed conditions, sustained extensive recession at the upstream side. The electrode surface was examined by SEM/EDX methods in an undisturbed (not polished) state. Figs. 19 and 20 (5000X) illustrate typical views of the upstream area. The vesicular surface consists of a framework of Cu metal (possibly partly melted) surrounding voids originally containing grains of W or containing pitted and recessed W. Although both metals obviously receded, the W appears to recede preferentially. Obviously, the upstream area was subjected to localized current concentration (arcing) and excessive heating. Cu-metal with superior thermal conductivity dissipated heat more rapidly than the W and the latter oxidized. The oxidation products either vaporized or, being poorly adherent, were swept or abraded off by the gas stream. The deep voids, sometimes retaining the vague hexagonal outline of the pre-existing W grains, may suggest oxidation/vaporization as the dominant process.



Interestingly, the downstream (presumably cooler) portion of the electrode surface consists of swarms of ridges and shallow valleys trending parallel with the direction of plasma flow. These originate near the vicinity of but not from within the upstream area of active metal recession. They terminate near the downstream edge of the anode. Fig. 21 (1000X) illustrates these features. The ridges (center and far left and right) consist of relatively undisturbed grains of W bonded by Cu. Within the valleys, the material consists of poorly bonded, almost loose, grains of W. Cu clearly is absent. These valleys may represent zones of lesser current concentration and heating, relative to the upstream area. They probably develop via oxidation of the Cu within a lower temperature regime. This would serve to weaken the cohesion among W grains which then would be subjected to ablation by the gas stream.

The observations above suggest that Cu/W anodes probably are not superior to pure Cu. The mechanical mixture of metals, indeed, may compromise the excellent thermal conductivity of copper alone.



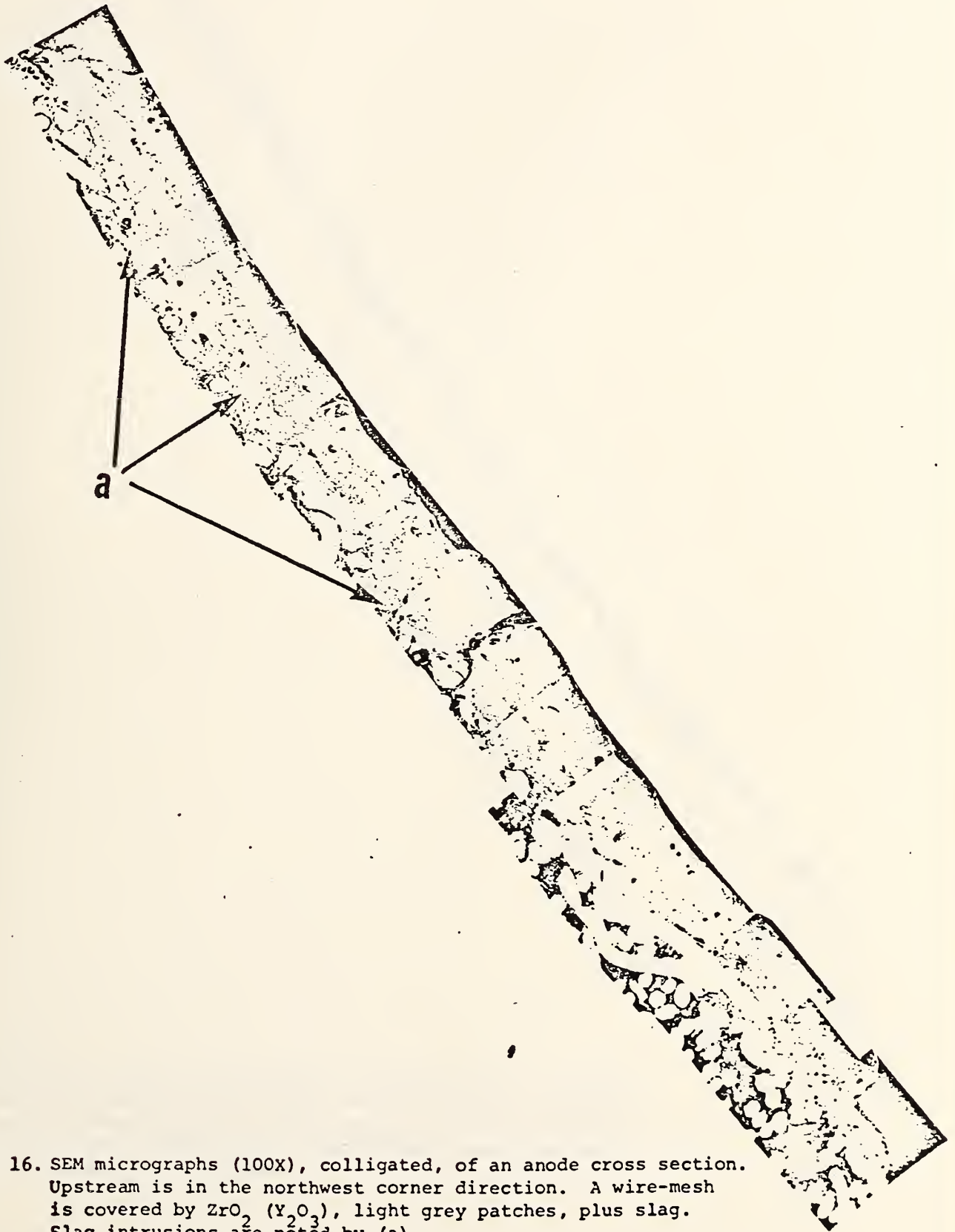


Fig. 16. SEM micrographs (100X), colligated, of an anode cross section. Upstream is in the northwest corner direction. A wire-mesh is covered by  $ZrO_2$  ( $Y_2O_3$ ), light grey patches, plus slag. Slag intrusions are noted by (a).



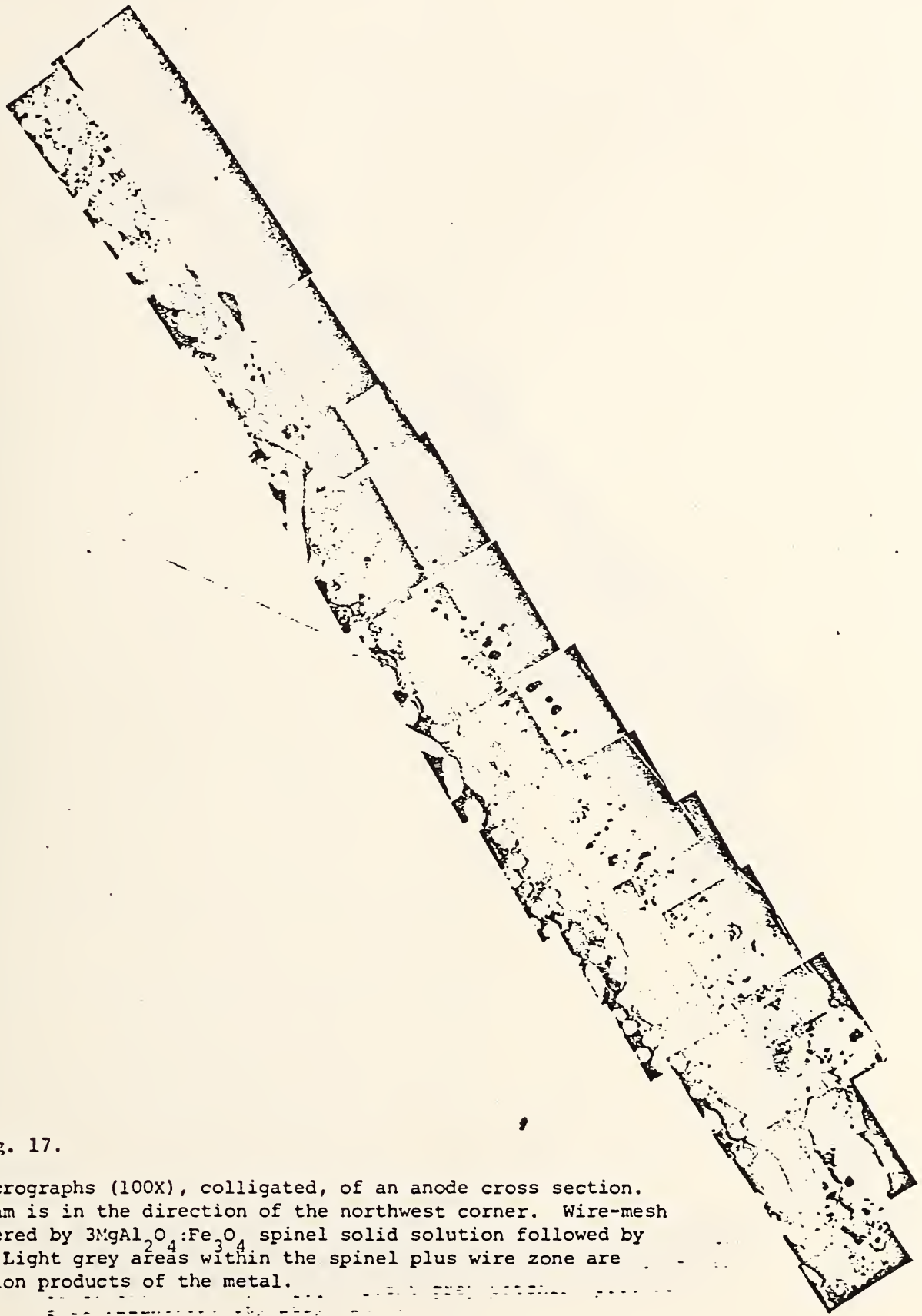


Fig. 17.

SEM micrographs (100X), colligated, of an anode cross section. Upstream is in the direction of the northwest corner. Wire-mesh is covered by  $3\text{MgAl}_2\text{O}_4:\text{Fe}_3\text{O}_4$  spinel solid solution followed by slag. Light grey areas within the spinel plus wire zone are oxidation products of the metal.

SEM INSTRUMENTS AND TECHNIQUES



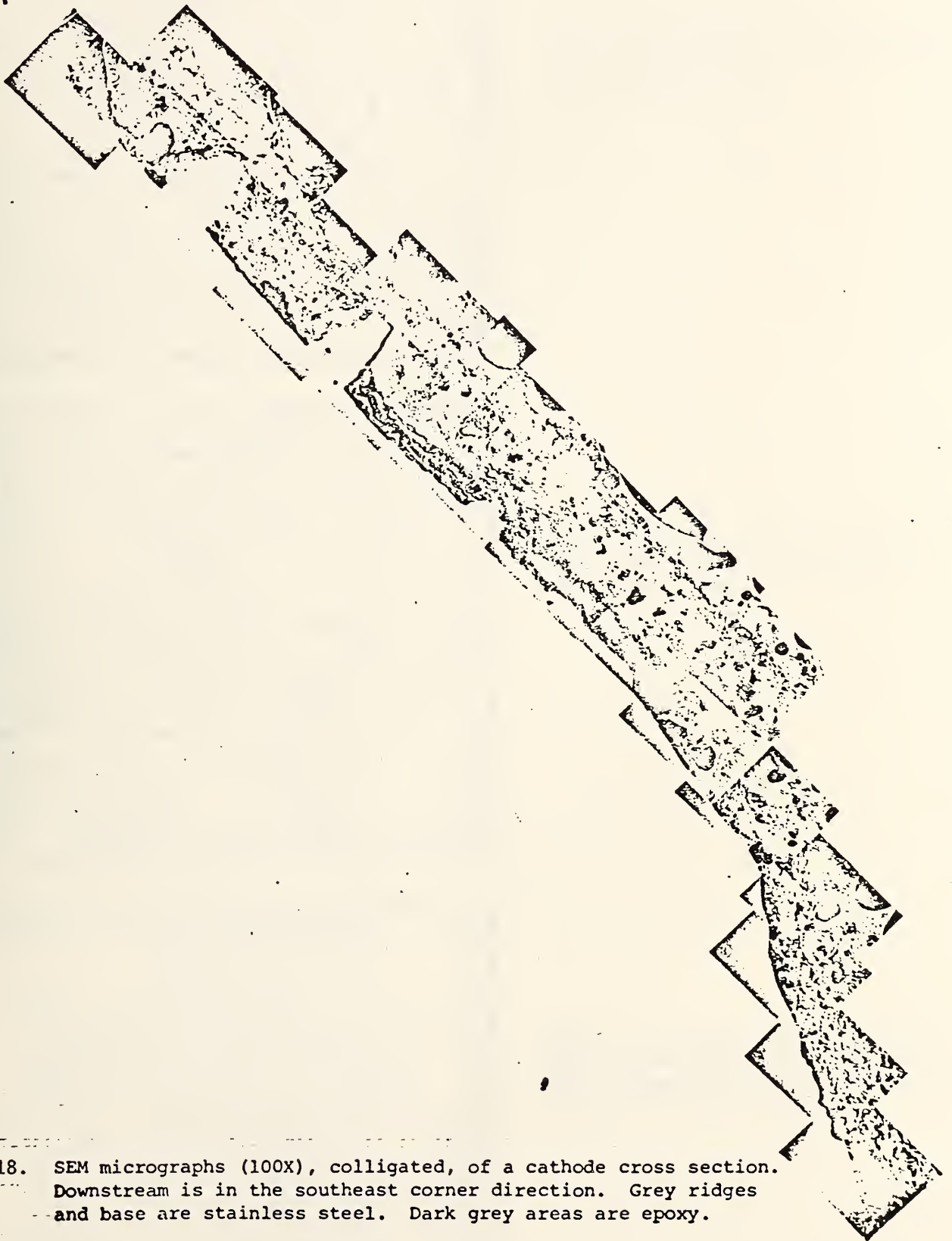


Fig. 18. SEM micrographs (100X), colligated, of a cathode cross section. Downstream is in the southeast corner direction. Grey ridges and base are stainless steel. Dark grey areas are epoxy.



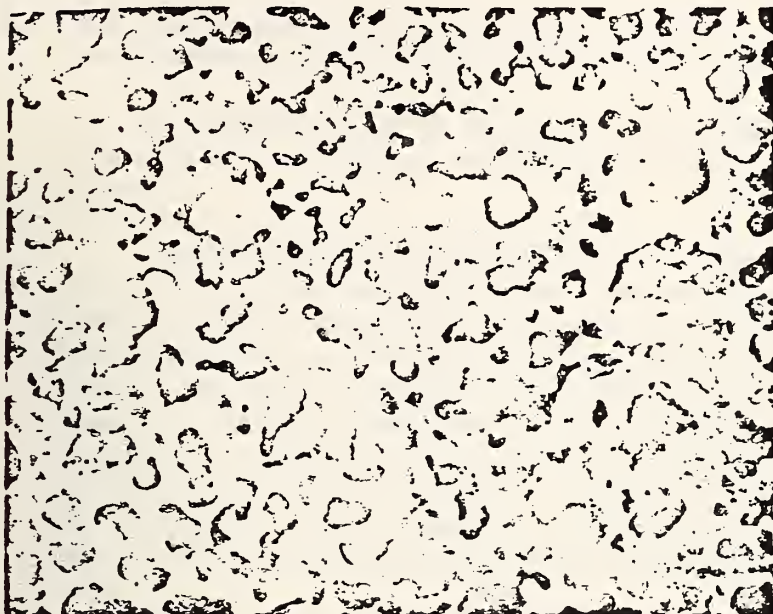


Figure 19. SEM micrograph (5000X), surface (unpolished) of Cu/W metal anode, upstream area.

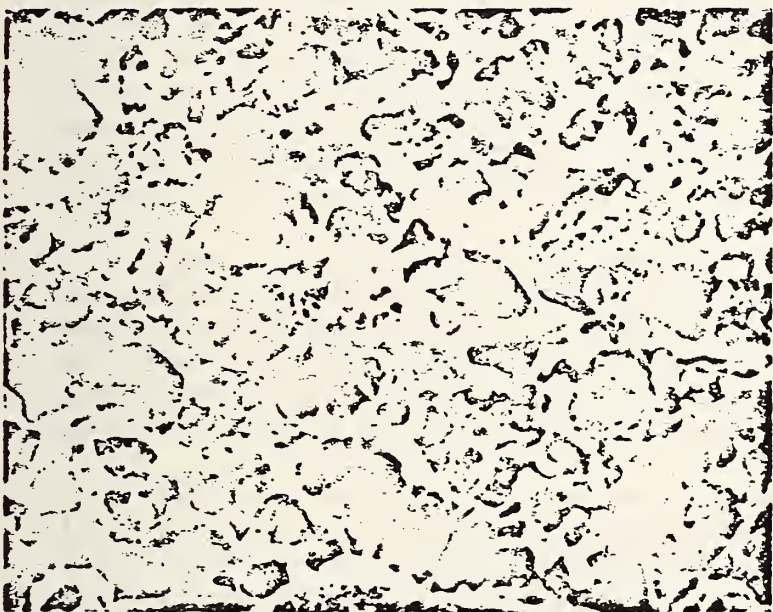


Figure 20. SEM micrograph (5000X), surface (unpolished) of Cu/W metal anode, upstream area.

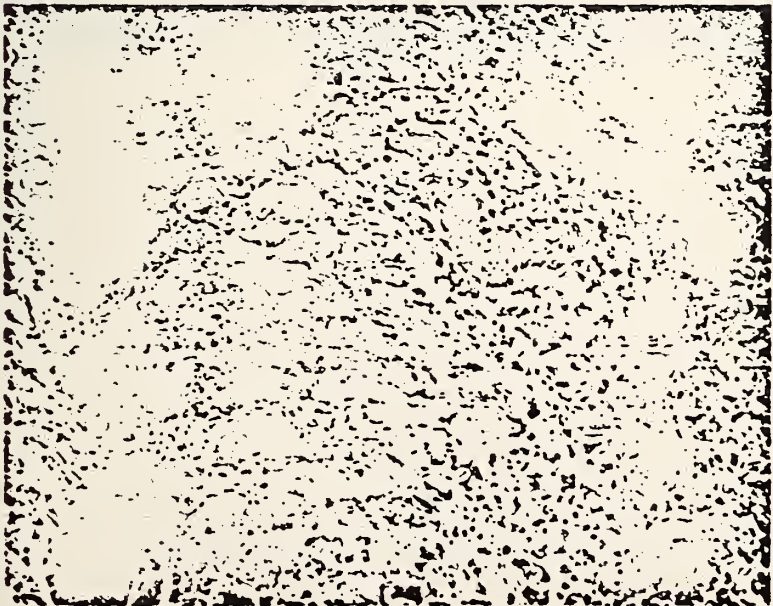


Figure 21. SEM micrograph (1000X), surface (unpolished) of Cu/W metal anode, downstream area consisting of a ridge and valley complex.



b. SEM Examination of Corhart X-317 Ceramics (Magnesia Spinel) Tested at the Fluidyne Engineering Corporation (E. N. Farabaugh)

Preheater material tested at Fluidyne was examined to determine elemental constituents, microstructure and the thickness of the reacted layers.

Specimen FN-90 (Corhart X-317) was cycled between 1800-1700 °K for 30 hours in the presence of ash and seed ( $K_2SO_4$ ). Fig. 22a is a 100X micrograph of part of this specimen. The change in microstructure defines the extent of the reacted layer. In this specimen this layer is ~0.5 mm thick. Elemental concentrations of Mg, Al, Si, Ca, K, Cr, and Fe were found in the reacted layer. At a distance of ~0.8 mm from the edge of the specimen, only Mg and Al could be observed in the EDX spectra. Fig. 22b is a Mg map of the same area. Note the Mg depleted reacted area. Fig. 22c is an Al map of the same area. Maps of Si, K, Ca, Cr, and Fe in the same area show concentrations of these elements in the upper layer.

Fig. 23a is a 100X micrograph taken of specimen FN-85. This specimen was cycled between 1800-1600 °K for 30 hours in the presence of seed ( $K_2CO_3$ ) but no ash. Figs. 23b and 23c are Mg and Al maps of the same area. Maps of K, Si, Fe and Ca distributions were also recorded. It is difficult from these maps and micrographs to determine precisely where the reacted area ends. Other SEM and EDX work has indicated a layer thickness of ~0.2 mm. This was determined by scanning from the edge in and observing the position where K and Fe concentrations fell to zero.

These two specimens are interesting. FN-90 was tested under conditions not different from FN-85. The results from the examination of these two specimens were quite similar. Both showed Mg deficient layers which could be explained by suggestions of preferential reaction of the MgO with the gas stream. Both had relatively thick reaction layers 0.4-0.5 mm. Elemental constituents were also the same in these two specimens.

FN-85 was the only X-317 magnesia spinel tested using  $K_2CO_3$  for seed. It is the only one, so far, which has had such a vague difference between the reacted layer and the bulk material. There is not the striking difference in Mg and Al maps as seen before. Also, the reacted layer is thinner ~0.2 mm. This layer thickness compares to that reacted layer of FN-70 (~0.2 mm) which was also tested in the absence of ash. It seems that the X-317 didn't react as much with the  $K_2CO_3$  seeded gas stream as with the  $K_2SO_4$  seeded streams.





Fig. 22a . 100X SEM micrograph of reacted layer of FN-90.



Fig. 22b. Mg map of the same area as 22a.

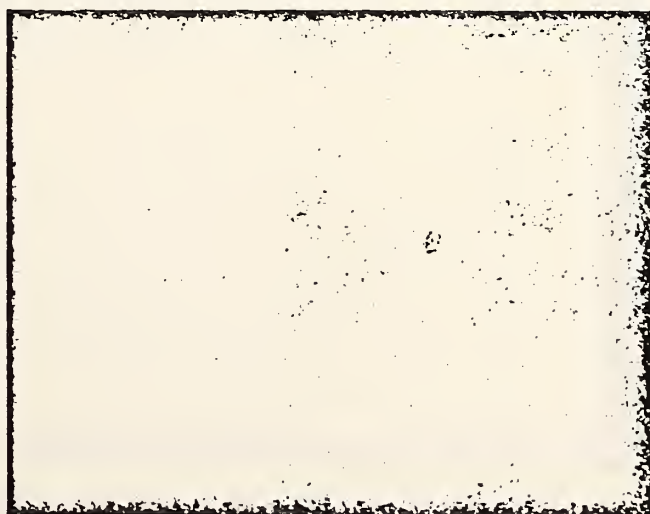


Fig. 22c. Al map of the same area as 22a .



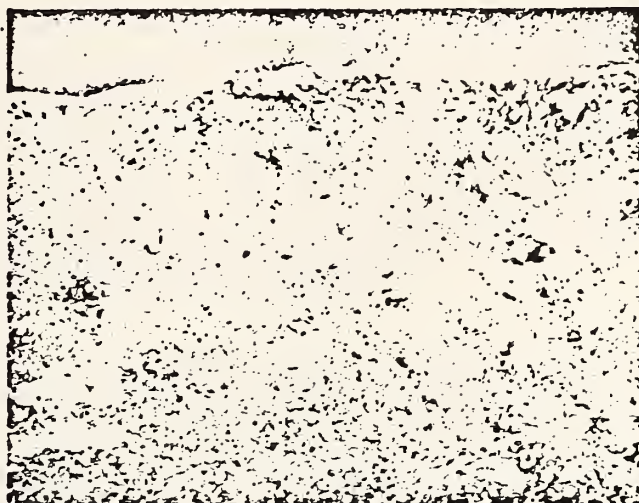


Fig. 23a. 100X SEM micrograph of reacted layer of FN-85.



Fig. 23b. Mg map of the same area as 23a.



Fig. 23c. Al map of the same area as 23a.



c. Joint US-USSR Test of Soviet Materials at UTSI (A. J. Armstrong)

From October 8-14, 1976 six runs were made at UTSI in the UTSI II MHD channel. A. J. Armstrong of NBS participated in the tests. Three runs were made with western Kentucky coal +  $K_2SO_4$  seed to produce an acid slag. Two additional runs were made with the same coal and seed but with added  $Ca(OH)_2$  to produce a basic slag. Finally, one run was made with kerosene alone and no seed. In general, a run would consist of up to 15 minutes of warm-up with kerosene followed by up to 60 minutes of operation with coal and seed. The coal containing runs subjected the materials to severe erosion, thermal shock and chemical attack.

The two Soviet materials tested ( $SiC + 7 \text{ wt.}\% Ti$  and  $60 \text{ wt.}\% LaCrO_3 + 40 \text{ wt.}\% Cr$ ) displayed high thermal shock resistance. Both materials seem to have suffered from erosion with the doped  $SiC$  apparently standing up best. The doped  $SiC$  appeared to show a large increase in chemical attack when subjected to the basic slag. These observations are from viewing the electrodes after sectioning and are preliminary to a more intense post-test examination now in progress at UTSI and IVTAN. A post-test analysis at NBS is planned upon receipt of samples from UTSI.

One U.S. (or NBS) material was included in two of these runs with acid slag. The material was dense sintered spinel ( $3MgAl_2O_4:Fe_3O_4$ ). Out of four samples tested only one was recovered. Failure seems to be due to thermal shock. The one sample recovered has many cracks and apparent erosion of 0.3-0.6 mm. Very little chemical attack by seed or slag has been detected to date.



Task L. ASSESSMENT OF STEAM PLANT COMPONENTS (J. R. Cuthill)

This is the sixth quarterly report since the initiation of Task L. Task L is concerned with the selection of commercially available alloys that appear to be promising materials for critical components in the downstream steam plant, and recommendations for further in-service testing.

The first critical component, and probably the most important on the basis of the quantity of material involved, is steam heat exchanger tubing. The requirement that distinguishes this MHD application from a conventional coal-fired steam plant is the severe hot corrosion anticipated due to the 1% potassium by weight in the flue gas which is currently predicted (1) to be almost entirely in the form of KOH and  $K_2SO_4$  with a small amount of KCl, (see Table 1). However, in assessing alloys in reference to this application, of necessity the hot corrosion results in  $Na_2SO_4/NaCl$  mixtures have been used as a guide. The marine gas turbine literature concerned with attack by  $Na_2SO_4/NaCl$  mixtures is relatively extensive whereas there is a surprising paucity of data on attack by  $K_2SO_4$  except for the investigations by the U.S. Bureau of Mines at Bruceton, PA (2) and by the Central Electricity Research Laboratories in England (3). Both of the latter studies have been discussed in previous quarterly progress reports. (See previous quarterly reports also for a discussion of the nature of the "hot corrosion" type of attack and the behavior of various alloy additions to attack by molten  $Na_2SO_4/NaCl$  mixtures). This marine gas turbine hot corrosion research has been considered a useful guide as a first approximation to attack by molten potassium salts on the basis that  $K_2SO_4/KCl$  mixtures are reported to behave much the same way as the  $Na_2SO_4 \cdot NaCl$  mixtures in the crucible tests (4,5). However, there are differences reported also. In a review on Corrosion in Fused Salts, D. Inman (6) reports that in the presence of air, NaCl produces greater attack than KCl but in the case of hydroxides just the reverse is observed; KOH produces greater attack than NaOH. This greater severity of attack by KOH in comparison with NaOH is shown in some data of the Gurloch (7) which is reproduced in Figs. 1a,b. A comparison of the weight loss in KOH vs. NaOH, for pure nickel, Kh18N9T\* stainless steel, and Armco iron is shown. (Compare Fig. 1a vs. 1b). An interesting implication of the data is that pure nickel resists this type of attack better than the stainless steel.

Fortunately, the predicted flue gas composition (see Table 1) has the KOH being converted to  $K_2SO_4$  in the steam superheater. The situation in the sulfate form looks appreciably better. Shirley (5) reports essentially the same attack on Nimonic 80A and F.C.B.(T) steel<sup>†</sup> in a  $K_2SO_4$ , 1% KCl mixture as in  $Na_2SO_4$ , 1% NaCl at 750 °C. However, Shirley's data showed the potassium salts, under the same conditions, as producing a 33% greater weight loss than the sodium salts, in the case of 337 stainless steel.

In view of these deviations between attack by potassium salts and by sodium salts a reasonably extensive search was made, therefore, to find just what data there was in the literature on attack by molten potassium salts. A search requested from the Smithsonian Science Information Exchange of reports on current research in their files, which covers the periods, FY'75, FY'76, and a portion of FY'77, revealed no on-going research on the attack of metals or alloys by molten  $K_2SO_4$ , KCl,  $K_2CO_3$ , KOH, or other potassium salts. Data

\* Kh18N9T steel: 18Cr, 9Ni, 1Ti.

† F.C.B.(T) steel: 17.5 Cr, 12 Ni, 1 Nb.



abstracted from references pertinent to a comparison of the corrosion attack by potassium salts vs. sodium salts, which were found by searching primarily the last ten years of chemical abstracts are summarized in Table 2.

It is evident that the data in the literature on the attack of commercial alloys by molten potassium sulfate, carbonate, chloride, or hydroxide is very incomplete. However, data from laboratory tests in any one of these potassium salts would be only a first order screening test because the interaction between the constituents is more than likely not only important but controlling.

This appears to be the case in marine gas turbine hot corrosion where pure  $\text{Na}_2\text{SO}_4$  does not produce serious attack, but combined with a small amount of  $\text{NaCl}$ , the rate of attack is increased many-fold. (See previous quarterly progress report on Task L for data and a discussion of  $\text{Na}_2\text{SO}_4 - \text{NaCl}$  hot corrosion attack). The chemistry of the MHD system flue gas is much more complex. The mol fractions of the principal constituents that STD Research Corp. predicts to be in the flue gas in the steam superheater is given in Table 1. Depending upon the exact amount of excess oxygen present in the flue gas, Reid (8) discusses how pyrosulfates and trisulfates could form and, in turn, be directly responsible for the heat exchanger tube attack in conventional coal-fired plants. Reid proposes (9) that the trisulfates  $\text{Na}_3\text{Fe}(\text{SO}_4)_3$  and  $\text{K}_3\text{Fe}(\text{SO}_4)_3$  are mainly responsible for the loss of metal from the superheater and reheater tubes at 1100 °F (600 °C) and above (metal wall temperatures). Note that this is the temperature range anticipated in the Baseline Plant design (see Fig. 2 reproduced from previous quarterly report, Sept. 30, 1976). In lower temperature regions, 600-900 °F range, (300-500 °C), Reid (10) discusses how the molten pyrosulfate,  $\text{K}_2\text{S}_2\text{O}_7$  could be present and likely to be responsible for hot corrosion attack. Note that  $\text{K}_2\text{SO}_4$  has a melting point of 1076 °C so is unlikely, in pure form, to be a factor in corrosion at these low wall temperatures. Carey, Cross and Reid (11) report that maintenance of oxidizing conditions near the tube wall reduced metal attack. They attributed this to the suppression of  $\text{SO}_3$  formation. The  $\text{SO}_3$  is required for pyrosulfate formation. However, oxidizing conditions must be maintained around the superheater tubes for another reason - to maintain the integrity of the protective oxide films on the alloy. For example, the 50 Ni - 50 Cr alloy (INCO 671) is probably one of the best alloys for resisting the hot corrosion attack. However, the atmosphere must be oxidizing to maintain the integrity of the  $\text{Cr}_2\text{O}_3$  protective film.

### Conclusions

The general conclusion to be drawn from the literature search is that the use of marine gas turbine hot corrosion research results as a guide to the selection of promising alloys for further in-service testing, as has been done in this series of quarterly reports, is valid. However, there are enough uncertainties in the complex chemistry of the MHD system to make in-service testing in a rig that simulates as closely as possible the MHD conditions necessary if one wants to determine the lowest cost alloy that will do the job.



## Future Plans

(1) As part of the literature search for data on corrosion attack by molten potassium salts, a computer search was made of the National Technical Information Service files. Some work of particular interest was turned up but the full reports have not been received as yet. These data will be reviewed in the next quarterly report.

(2) Data on the hard facing coatings and alloy overlaps, to resist wear, as well as hot corrosion attack, will be compiled.

## References

1. Baseline Plant System Design Description, Joint Report-Gilbert Associates and STD Research Corp., June 1976.
2. D. Bienstock, R. J. Demski and R. C. Covey, Corrosion of Heat-Exchange Tubes in a Simulated Coal-Fired MHD System, J. of Eng. for Power (ASME Trans.) 93, 249 (1971).
3. J. B. Heywood and C. J. Womack, "Open-Cycle MHD Power Generation", Chapter 10, Pergamon Press, Oxford, 1969.
4. John Stringer, Hot Corrosion in Gas Turbines, MCIC Report #72-08, Battelle Columbus, 1972.
5. H. T. Shirley, Effect of Sulfate-Chloride Mixtures in Fuel-Ash Corrosion of Steels and High-Nickel Alloys, J. Iron and Steel Inst. 182
6. D. Inman, Corrosion in Fused Salts, Chap. 2.10, Corrosion, Vol. I, L. L. Shrier, ed., Newnes-Butterworths, London, 2nd ed., 1976.
7. E. I. Gurovich, Effects of Fused Lithium, Sodium and Potassium Hydroxides on Nickel, Copper, Iron and Stainless Steel, Zh. Grikl. Khim. 33, 836-40 (1959), (English Translation).
8. W. T. Reid, External Corrosion and Deposits, Boilers and Gas Turbines, American Elsevier Publising Co., 1971.
9. *ibid*, p. 125.
10. *ibid*, p. 104.
11. R. C. Carey, B. J. Cross and W. T. Reid, External Corrosion of Furnace-Wall Tubes-II Significance of Sulfate Deposites and Sulfur Trioxide in Corrosion Mechanism, ASME Trans. 67, 289 (1945).
12. H. Arup, N. Korsgard, D. Hansen, Stress Corrosion Cracking of Au Stainless Steel in Potassium Hydroxide at Elevated Pressures and Temperatures, Proceedings of the 6th Scand. Corros. Congr., Sweden Corros. Inst. Stockholm, 1971, p. 22
13. N. D. Tomashov and N. I. Tugarinav, Mechanism of Corrosion of Metals in Molten Chlorides, p. 1681-7 (1956), English Translation.



Table 1

Principal Constituents in Flue Gas Through Steam Heat-Exchanger (from Ref. 1).

Molecular Specie	Mole Fraction		
	entering* superheater	entering* reheater	leaving* reheater
CO	.00010	--	--
CO <sub>2</sub>	.17212	.17269	.17212
H <sub>2</sub> O	.08888	.09095	.09102
K	.00005	--	--
KCl	.00004	.00004	.00004
KOH	.00366	.00011	--
K <sub>2</sub> SO <sub>4</sub> (l)	.00184	.00365	--
K <sub>2</sub> SO <sub>4</sub> (s)	--	--	.00371
N <sub>2</sub>	.72077	.72285	.72293
O <sub>2</sub>	.00093	.00004	.00001
SO <sub>2</sub>	.00253	.00073	.00067

\*See Fig. 2, Schematic of Baseline Plant Design, reproduced from previous (5th) Quarterly Progress Report.



Table 2

Data From Pertinent References on Attack of Metal and Alloys by Potassium Salts vs. Sodium Salts.

$K_2SO_4$ -KCl vs.  $Na_2SO_4$ -NaCl

Ref. 5:

<u>Contact Mixture,</u> <u>750 °C</u>	<u>Wt loss, mg/cm<sup>2</sup></u>		<u>Nimonic 80A*</u>
	<u>337 steel*</u>	<u>F.C.B.(T) steel*</u>	
99% $Na_2SO_4$ , 1% NaCl	11,12,4	14,13,12	34,34,53
99% $K_2SO_4$ , 1% KCl	16	13	31

\*337: 16Cr,18Ni,7Co,3Mo,3Cu,1Ti, bal. Fe; \*F.C.B.(T): 18Cr,12Ni, bal.Fe;  
\*Nimonic 80A: 75Ni,20Cr, bal. Fe.

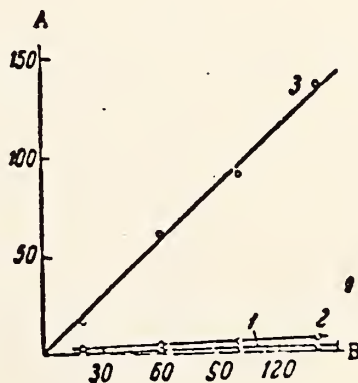
KOH vs. NaOH

Ref. 7: KOH may be up to 20 times as corrosive as NaOH in respect to 18-8 type stainless steels. See Fig. .

Ref. 12: KOH pellets placed in the bottom of U-bond stress corrosion specimens caused cracking in 18-8 stainless steels but not in 2.25 Cr, 1 Mo steel at 310-400 °C. The moisture content appears to be critical and there is indication that 0.05 mol% or more of  $CO_2$  inhibits cracking in the presence of the KOH.

KCl vs. NaCl

Ref. 13:



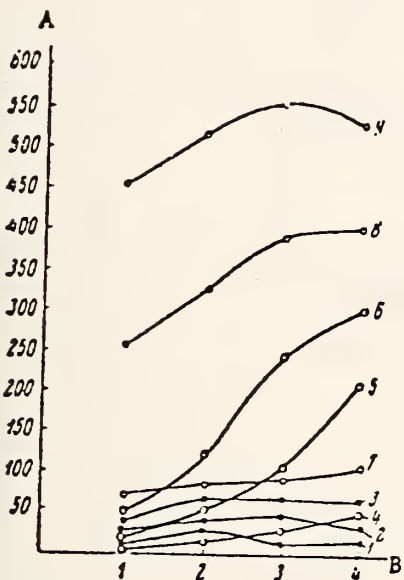
Corrosion of Fe in different chlorides at temperatures 70°C above the melting point of the chloride.

A) Corrosion activity K (in g/m<sup>2</sup>).

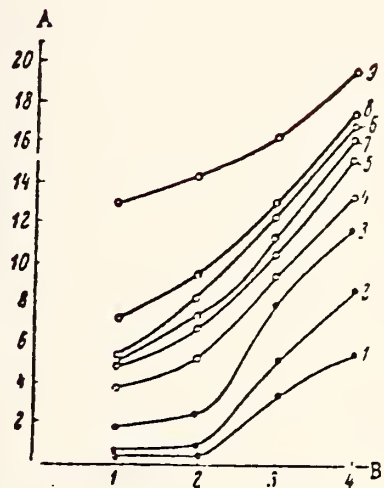
B) time  $\tau$  (in minutes).

Curves: 1) NaCl; 2) KCl; 3)  $CaCl_2$ .





(a) Isotherms for corrosion in fused KOH: A) corrosion (in  $\text{g}/\text{m}^2$ ); B) duration of experiment (hours); nickel: 1) 500°; 2) 450°; 3) 400°; Kh18N9T steel: 4) 400°; 5) 450°; 6) 500°; "Armco" Iron: 7) 500°; 8) 400°; 9) 450°.



(b) Isotherms for corrosion in fused NaOH: A) corrosion (in  $\text{mg}/\text{m}^2$ ); B) duration of experiment (hours). Nickel: 1) 350°; 2) 400°; 3) 450°; "Armco" Iron: 4) 350°; 5) 400°; Kh18N9T steel: 7) 350°; 8) 400°; 9) 450°.

Fig. 1a,b. Corrosion attack in Molten KOH vs NaOH (from Ref. 7)



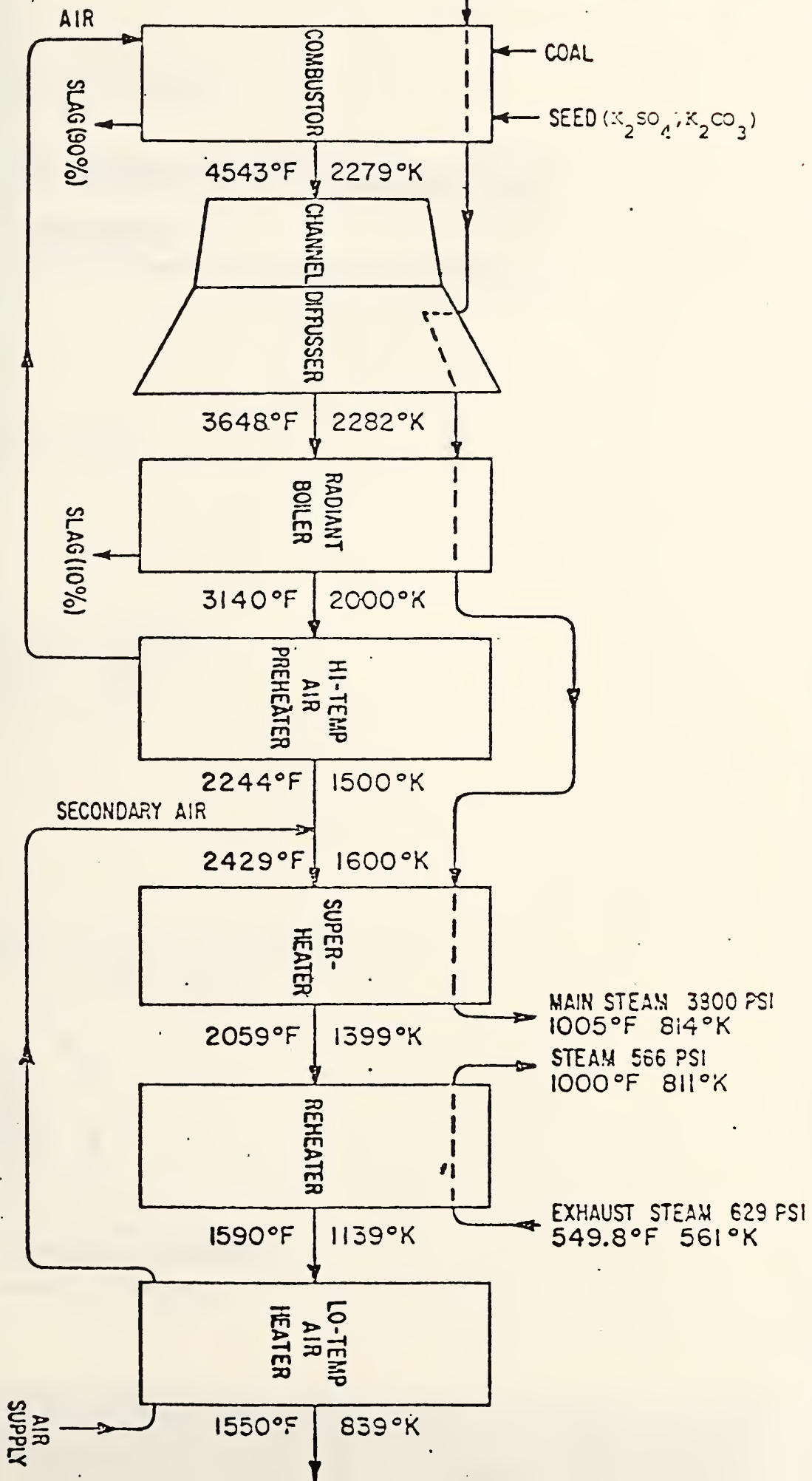


Figure 2. Baseline Reference Design for an Open Cycle MHD Power Plant.

